Direct binding of arsenicals to nuclear transport factors disrupts nucleocytoplasmic transport

Emma Lorentzon[1], Jongmin Lee[2], Jakub Masaryk[1], Katharina Keuenhof[1], Nora Karlsson[1], Charlotte Galipaud[1], Rebecca Madsen[1], Johanna L. Höög[1], David E. Levin[2], and Markus J. Tamás[1,*]

[1]Department of Chemistry and Molecular Biology, University of Gothenburg, Box 462, S-405 30 Göteborg, Sweden

[2]Department of Molecular and Cell Biology, Boston University Henry M. Goldman School of Dental Medicine, Boston, MA, USA

Running title: Arsenic disrupts nucleocytoplasmic transport

*Corresponding author: Markus J. Tamás, Department of Chemistry and Molecular Biology, University of Gothenburg, S-405 30 Göteborg, Sweden, Tel: +46-31-786 2548; Fax: +46-31-786 3910; Email: markus.tamas@cmb.gu.se

Key words: arsenic, karyopherin, nuclear pore protein, nuclear pore complex, nuclear import, nuclear export, nuclear envelope

ABSTRACT

Human exposure to arsenicals is associated with devastating diseases such as cancer and neurodegeneration. At the same time, arsenic-based drugs are used as therapeutic agents. The ability of arsenic to directly bind to proteins is correlated with its toxic and therapeutic effects highlighting the importance of elucidating arsenic-protein interactions. In this study, we took a proteomic approach and identified 174 proteins that bind to arsenic in *Saccharomyces cerevisiae*. Proteins involved in nucleocytoplasmic transport were markedly enriched among the arsenic-binding proteins, and we demonstrate that arsenic-binding to nuclear import factors results in their relocation from the nuclear envelope and subsequent aggregation in the cytosol. Similarly, nuclear pore proteins that make up the nuclear pore complex mislocalized and aggregated in arsenic-exposed cells. Consequently, arsenic was shown to inhibit nuclear protein import and export. We propose a model in which arsenic-binding to nuclear transport factors leads to their mislocalization and aggregation, which disrupts nucleocytoplasmic transport and causes arsenic sensitivity.

INTRODUCTION

Human exposure to the poisonous metalloid arsenic is a global health threat that affects hundreds of millions of people (Chen and Costa, 2021). High concentrations of arsenic in the groundwater have been measured in a large number of countries and long-term exposure is associated with numerous human health problems such as skin disorders, cardiovascular disease, diabetes, cancers of the liver, lung and kidneys, and neurological and neurodegenerative disorders (Chen and Costa, 2021; Rahman et al., 2021; Wysocki et al., 2023). At the same time, arsenic-containing compounds are currently used in anticancer and antiparasitic therapy (Paul et al., 2023).

Pentavalent arsenate, As(V), and trivalent arsenite, As(III) are the most common forms of inorganic arsenic in the environment (Chen and Costa, 2021) and once inside cells, inorganic arsenic can be enzymatically converted into mono-, di-, and trimethylated metabolites (Thomas, 2021). Various forms of arsenic affect cells and living organisms in distinct ways. Due to its chemical similarity to phosphate, As(V) competes with phosphate in biochemical reactions and disrupts adenosine triphosphate (ATP) production. As(III) has high affinity for sulfhydryl groups, such as the thiol groups of cysteine residues, and binding of As(III) and its metabolites to proteins can disrupt protein conformation, function, and interactions (Chen et al., 2019; Kitchin and Wallace, 2008; Shen et al., 2013; Tamás et al., 2014; Vergara-Geronimo et al., 2021; Wysocki et al., 2023). Methylation affects the toxicity of arsenicals as well as their modes of action and protein binding specificities (Shen et al., 2013; Thomas, 2021). For example, As(III) can bind up to three cysteine residues, monomethylarsenite [MAs(III)] can bind two cysteine residues and dimethylarsenite [DMAs(III)] can bind only one cysteine residue (Shen et al., 2013). Arsenic's ability to bind to proteins is associated with its toxicity, but also with its therapeutic effects. For instance, binding to cysteine residues in the oncoprotein PML-RARα underlies the anticancer activity of arsenic trioxide in patients with acute promyelocytic leukaemia (APL) (Lallemand-Breitenbach et al., 2008; Zhang et al., 2010). Similarly, arsenic-binding to specific kinases and transcriptional regulators is linked to arsenic resistance in yeast and bacteria (Guerra-Moreno et al., 2019; Kumar et al., 2016; Shi et al., 1994). While the toxicity of trivalent arsenite has traditionally been attributed to its interactions with sulfhydryl groups in native (folded) proteins (Kitchin and Wallace, 2008; Shen et al., 2013), recent studies have shown that As(III) also targets non-native proteins impairing their proper folding (Hua et al., 2022; Jacobson et al., 2012; Ramadan et al., 2009; Sapra et al., 2015). In cells, this results in extensive protein misfolding and aggregation which, in turn, has a negative effect on cell proliferation and viability (Andersson et al., 2021; Hua et al., 2022; Ibstedt et al., 2014; Jacobson et al., 2012).

Thus, knowledge of arsenic-protein interactions is key to understand the toxic and therapeutic effects of arsenicals as well as cellular sensing and defence mechanisms. To this end, several large-scale

74 studies have been performed with the aim to identify arsenic-binding proteins (Liu et al., 2023). For
75 example, 360 proteins bound to arsenic *in vitro* using a human proteome microarray (Zhang et al.,
76 2015a) and *in vivo* studies identified 40 arsenic-binding proteins in APL cells (Zhang et al., 2015b), 50
77 proteins in human breast cancer cells (MCF-7 cell line) (Zhang et al., 2007), 51 proteins in human
78 embryonic kidney epithelial cells (HEK293T) (Dong et al., 2022), and 48 proteins in A549 human lung
79 carcinoma cells (Yan et al., 2016). Follow-up experiments indicated that some of these proteins are
80 *bona fide* targets of arsenic-binding and inhibition (Yan et al., 2016; Zhang et al., 2015a; Zhang et al.,
81 2015b). While identifying the arsenic-binding proteome is a promising approach to address toxicity
82 and resistance mechanisms, the aforementioned *in vivo* studies identified relatively few targets and a
83 comprehensive catalogue of *in vivo* arsenic-protein interactions and the resulting consequences on cell
84 physiology is still lacking.

85 In this study, we took a proteomic approach and identified 174 proteins that bind to arsenic in budding
86 yeast *Saccharomyces cerevisiae*. Proteins involved in nucleocytoplasmic transport were strongly
87 enriched among the arsenic-binding proteins, and data from follow-up experiments is consistent with
88 a model in which arsenic-binding to nuclear transport factors leads to their mislocalization and
89 aggregation, which disrupts protein transport across the nuclear envelope and causes arsenic
90 sensitivity.

91

92 **RESULTS**

93 **Proteome-wide identification of arsenic-binding proteins in yeast.**

94 To identify proteins that bind to arsenic *in vivo*, we took an unbiased proteomic approach in *S.*
95 *cerevisiae* using biotin-conjugated As(III) (hereafter As–biotin) as a probe (Kumar et al., 2016; Lee and
96 Levin, 2019). We previously noted that As-biotin cannot discriminate between As(III)-binding proteins
97 and proteins that bind to MAs(III) due to intracellular conversion of As(III) into MAs(III) (Lee and Levin,
98 2018; Lee and Levin, 2019). Therefore, we incubated yeast cells that lack the methyltransferase
99 enzyme Mtq2 responsible for As(III) methylation (Lee and Levin, 2018) with 50 µM As–biotin without
100 or with a 10 min pretreatment with 1 mM As(III) or 500 µM MAs(III) as blocking agents (Fig. 1A): the
101 pretreatments were performed to get an indication of which arsenical binds to each protein as binding
102 of As-biotin to a protein is expected to be attenuated in the presence of As(III) or MAs(III), and *mtq2Δ*
103 cells were used to avoid metabolism of the blocking arsenical (Kumar et al., 2016; Lee and Levin, 2018;
104 Lee and Levin, 2019; Lee and Levin, 2022). After cell disruption and As-biotin pull-down with
105 streptavidin-agarose beads, candidate arsenic-binding proteins were eluted, separated by SDS-PAGE
106 electrophoresis, and identified by microcapillary liquid chromatograph-tandem mass spectrometry
107 (LC/MS/MS) (Fig. 1A). As a control, we performed pull-downs using cells that had not been incubated
108 with As-biotin. In total, 776 proteins were identified in at least one of the conditions (Supplementary
109 Table S1). To select candidate arsenic-binding proteins, we filtered the 776 proteins using the following
110 criteria: (1) no peptide present in the control, (2) ≥5 unique peptides identified after As-biotin pull-
111 down, and (3) ≥2-fold reduction of signal/peptide intensity when competitor As(III) or MAs(III) was
112 present during pull-down. Applying these stringent filtering criteria gave a list of 174 candidate arsenic-
113 binding proteins (Table S2). To our knowledge, this represents the largest set of *in vivo* arsenic-binding
114 proteins reported to date.

115 Several of the 174 yeast proteins have human orthologues that were previously reported to bind to
116 arsenic in large-scale *in vitro* and *in vivo* screens (Dong et al., 2022; Zhang et al., 2015a; Zhang et al.,
117 2007) including subunits of the chaperonin TRiC/CCT complex involved in protein folding, metabolic
118 enzymes such as glycerol-3-phosphate dehydrogenase, aldehyde dehydrogenase and members of the
119 pyruvate dehydrogenase complex, proteins involved in DNA replication including components of the
120 minichromosome maintenance (MCM) complex, α- and β-tubulin, and ribonucleotide reductase
121 implicated in DNA synthesis and repair. Thus, these proteins may represent evolutionarily conserved
122 arsenic-binding targets. Of these, the chaperonin TRiC/CCT (Pan et al., 2010), tubulin (Zhang et al.,
123 2007), and pyruvate dehydrogenase (Bergquist et al., 2009; Peters et al., 1946) have been proposed to
124 be direct toxicity targets.

125 The majority of the 174 proteins (103 proteins, 59%) had ≥2-fold reduced signal/peptide intensity in
126 the presence of As(III) as well as MAs(III), suggesting that they may bind both arsenicals (Table S2). 48
127 proteins (28%) reached the threshold of ≥2-fold reduction in signal/peptide intensity only in presence
128 of MAs(III) while 23 (13%) reached the threshold only in presence of As(III), suggesting that these
129 proteins preferentially bind to either MAs(III) or As(III), respectively. As(III) and MAs(III) preferentially
130 bind to the thiol group of cysteine residues in proteins (Kitchin and Wallace, 2008; Shen et al., 2013;
131 Zhang et al., 2015a), and virtually all 174 proteins (99.4%) contained at least one cysteine compared
132 to 90.7% in the yeast proteome ($P<10^{-7}$) (Fig. 1B). The arsenic-binding set was also significantly
133 enriched for proteins with cysteines adjacent or proximal to other cysteines (CC, CxC, CxxC and CxxxC
134 motifs), and the mean number of cysteines and CC motifs per protein was significantly higher in
135 arsenic-binding proteins compared to the proteome (Fig. 1B). Additionally, we observed a significant
136 overlap between the arsenic-binding proteins and a set of 145 yeast proteins that possess surface-
137 exposed reactive cysteines (12 proteins, P=0.0002) (Marino et al., 2010) (Fig. 1C). As(III) has been
138 shown to bind to proteins containing zinc finger motifs, specifically to C3H1 and C4 motifs (Vergara-
139 Geronimo et al., 2021; Zhou et al., 2011). 12 of the 174 proteins (P=0.11) in our dataset are putative
140 zinc-binding proteins of which 8 are predicted to contain C3H1 and C4 motifs (Wang et al., 2018). In
141 sum, the As-biotin probe identified proteins that bind to As(III) and MAs(III) or both arsenicals, and our
142 findings reinforce the strong preference of As(III)/MAs(III) for cysteine residues in proteins *in vivo*.

143

144 **Protein binding as a possible toxicity mechanism.**

145 It has been postulated that trivalent arsenic causes toxicity via protein binding, inactivating or
146 depleting important cellular functions (Chen et al., 2019; Kitchin and Wallace, 2008; Shen et al., 2013;
147 Tamás et al., 2014; Vergara-Geronimo et al., 2021; Wysocki et al., 2023). However, only few direct
148 toxicity targets and mechanisms have been described to date. One way to pinpoint candidate toxicity
149 targets is to perform drug-induced haploinsufficiency profiling (HIP) assays (Giaever et al., 1999; Lum
150 et al., 2004). A previous yeast HIP study identified 33 As(III) sensitive heterozygous diploid knockout
151 mutants (Pan et al., 2010) of which 8 encode proteins that were present in the arsenic-binding set
152 ($P<10^{-6}$) (Fig. 1D) including components of TRiC/CCT (Cct1, Cct4, Cct5, Cct7), α-tubulin (Tub3), the
153 nuclear pore protein Nup145, adenine-requiring Ade12, and the serine palmitoyltransferase Lcb1.
154 These proteins may represent *bona fide* arsenic toxicity targets, as proposed for TRiC/CCT (Pan et al.,
155 2010) and tubulin (Zhang et al., 2007).

156 Another way to identify direct toxicity targets is to integrate chemical-genetic and genetic interaction
157 data (Parsons et al., 2004). For this, we retrieved negative genetic interactors of selected arsenic-
158 binding proteins and asked whether the sets of negative genetic interactors are enriched for As(III)

159 sensitive mutants. Indeed, we observed significant enrichments in As(III) sensitivity among negative
160 genetic interactors of selected arsenic-binding protein-encoding genes involved in transport across the
161 nuclear envelope (*KAP121/PSE1* (P=0.0004), *NUP84* ($P<10^{-20}$)), components of TRiC/CCT (*CCT1* ($P<10^{-}$
162 ^{13}), *CCT5* ($P<10^{-7}$)), the alpha subunit of pyruvate dehydrogenase *PDA1* ($P<10^{-13}$), the translation
163 regulator *GCN20* (P=0.004), and the serine palmitoyltransferase *LCB1* (P=0.0002) (Fig. S1). Thus, the
164 tested arsenic-binding proteins might represent *bona fide* toxicity targets, as proposed for TRiC/CCT
165 (Pan et al., 2010) and pyruvate dehydrogenase (Bergquist et al., 2009; Peters et al., 1946).

166 We noted that a substantial fraction of the arsenic-binding proteins is essential for cell viability (73
167 proteins, 42%, $P<10^{-12}$) (Fig. 1E), suggesting that arsenic-binding might drain the active pool of these
168 essential proteins, resulting in poor growth or survival of yeast cells during arsenic stress. The set of
169 essential arsenic-binding proteins included proposed toxicity targets such as TRiC/CCT (Pan et al., 2010)
170 and tubulin (Zhang et al., 2007) and novel candidate targets such as proteins involved in
171 nucleocytoplasmic transport (Fig. S1; see further).

172 One way arsenic binding affects protein function is by interfering with their folding, thereby preventing
173 proteins from reaching their native fold and hence, their active conformation (Andersson et al., 2021;
174 Hua et al., 2022; Ibstedt et al., 2014; Jacobson et al., 2012). We found a significant overlap between
175 the set of arsenic-binding proteins and a set of 143 proteins that aggregated in As(III)-exposed yeast
176 cells (27 proteins, $P<10^{-16}$) (Ibstedt et al., 2014; Jacobson et al., 2012) (Fig. 1F), suggesting that arsenic-
177 binding to these proteins results in their misfolding and aggregation.

178 In sum, our findings suggest that a large fraction of the 174 arsenic-binding proteins identified here
179 may represent *bona fide* toxicity targets and support the notion that protein binding is a major arsenic
180 toxicity mechanism, by affecting protein folding and/or activity. Thus, integrating arsenic-protein
181 binding data with other datasets is a powerful approach to identify novel toxicity targets.

182

183 **Arsenic binds to proteins involved in nucleocytoplasmic transport.**

184 We next addressed if specific categories of protein functions are overrepresented among the arsenic-
185 binding proteins. Gene ontology (GO) analysis revealed that this set was enriched in processes
186 associated with protein import into the nucleus, chaperonin-mediated protein folding, carboxylic acid
187 metabolic processes, nuclear pore localization and organization, DNA unwinding involved in DNA
188 replication, tRNA transport, methylation and aminoacylation, and sphingosine and long-chain fatty
189 acid metabolism (Fig. 2A). Remarkably, the set of arsenic-binding proteins was markedly enriched for
190 functions in nucleocytoplasmic transport and included 8 out of the 11 importins (Kap104, Kap114,
191 Kap122, Kap123, Kap121/Pse1, Sxm1/Kap108, Nmd5/Kap119, Mtr10/Kap111) present in *S. cerevisiae*,

192 several exportins (Cse1/Kap109, Crm1/Kap124, Msn5/Kap142), and numerous nuclear pore proteins
193 (Nup84, Nup85, Nup120, Nup133, Nup145, Nup157, Nup170, Nup188, Nup192) (Table S2). This strong
194 enrichment together with our genetic analyses above implicating some of these proteins as direct
195 toxicity targets (Nup145, Nup84, Kap121/Pse1), raised the possibility that nucleocytoplasmic transport
196 is a key target of arsenic in living cells.

197 Importins are nuclear transport factors that bind to cargo proteins containing nuclear localization
198 signals (NLS) in the cytoplasm and facilitate their passage through the nuclear pore complex (NPC) into
199 the nucleus, exportins mediate the export of cargo proteins back to the cytoplasm, while nuclear pore
200 proteins (Nups) constitute the NPC (Aitchison and Rout, 2012; Wing et al., 2022). Importins and
201 exportins belong to the karyopherin (Kap) family of nuclear transport factors. While most karyopherins
202 can bind to their cargos directly (karyopherin β), in the case of the heterodimeric α/β complex, it is
203 karyopherin α that binds to the cargo with karyopherin β stabilizing/enhancing this interaction
204 (Aitchison and Rout, 2012; Wing et al., 2022). To validate arsenic-binding to selected importins
205 (karyopherin βs Kap123, Kap121/Pse1, Sxm1/Kap108), exportins (karyopherin βs Crm1/Kap124,
206 Msn5/Kap142) and Nups (Nup84, Nup188), we either introduced plasmids that expressed HA-tagged
207 versions of the corresponding genes into yeast cells or used cells that harboured GFP-tagged versions
208 of the genes in their genomes, and performed As-biotin pulldown assays. All tested proteins bound to
209 As-biotin and this binding was attenuated to various degrees in the presence of competitor As(III) or
210 MAs(III) (Figs. 2B, 2C). Thus, these proteins directly bind arsenic *in vivo* in form of As(III) and/or MAs(III).
211 We also chose to test arsenic-binding to the karyopherin α Srp1/Kap60 and the karyopherin β Kap95
212 even though they were not present in the hit list (no peptides were found for Srp1/Kap60 while Kap95
213 was below the threshold), because these proteins constitute the heterodimeric α/β complex that plays
214 a key role in nuclear transport of NLS-containing proteins in yeast (Aitchison and Rout, 2012). Kap95
215 readily bound to As-biotin and this binding was unaffected by competitor As(III) but clearly attenuated
216 in the presence of MAs(III) (Fig. 2C). Thus, Kap95 binds to arsenic in form of MAs(III) *in vivo*. In contrast,
217 Srp1 did not bind to As-biotin (Fig. 2B).

218 Most of the tested proteins (Sxm1, Kap95, Kap121/Pse1, Msn5, Nup84, Nup188) have adjacent or
219 proximal cysteines in their primary sequence (Fig. 2D). Analyses of their known or predicted 3D
220 structures revealed that most of these proteins contain cysteine pairs within approximately 5Å of each
221 other (Fig. S2), making them suitable substrates for As(III)/MAs(III) in their native folded structures. In
222 contrast, Kap123 and Crm1 lack adjacent or proximal cysteines in their primary sequence, raising the
223 question of how As(III) and/or MAs(III) bind to these proteins. Inspection of their 3D structures
224 revealed the presence of proximal cysteines that could potentially serve as binding sites in both
225 proteins (Fig. S2). Finally, Srp1/Kap60 does not have cysteine motifs in its primary sequence and the

226 closest cysteines in its 3D structure are separated by approximately 10Å with the thiol groups pointing
227 in opposite directions (Fig. S2), explaining why this protein is a poor substrate for As(III)/MAs(III).

228

229 **Importins mislocalize and aggregate in As(III)-exposed cells.**

230 Having established that arsenic binds to individual importins, we next addressed the consequence(s)
231 of this binding. First, we monitored the localization of chromosomally integrated Kap95-GFP. We chose
232 to focus on Kap95 because: (1) it plays a central role in nuclear transport of NLS-containing proteins in
233 yeast (Aitchison and Rout, 2012), (2) integration of chemical-genetic and genetic interaction data
234 suggested that Kap95 may be a direct arsenic toxicity target (Fig. S1), and (3) the human orthologue of
235 Kap95, Importin 90/KPNB1, was identified as a candidate arsenic-binding protein in MCF-7 cells (Zhang
236 et al., 2007). In untreated (control) cells, chromosomally integrated Kap95-GFP localized around the
237 yeast nuclear envelope (NE) (Fig. 3A, 3B). In As(III)-exposed cells, NE localization of Kap95-GFP was
238 disrupted and the protein was instead found in distinct foci that were dispersed throughout the cytosol
239 in the majority of cells (Figs. 3A, 3B). Cytosolic Kap95-GFP foci were also formed when the translation
240 inhibitor cycloheximide (CHX) was added at the same time as As(III) (Fig. 3B), suggesting that As(III)
241 impacts the localization of the native (folded) form of Kap95. Kap95 forms a heterodimeric nuclear
242 transport receptor together with Srp1 (Aitchison and Rout, 2012). As for Kap95, As(III) stress altered
243 the distribution of chromosomally integrated Srp1-GFP from the NE to distinct cytosolic foci (Fig. 3A)
244 both in the absence and presence of CHX (Fig. S3A), which is consistent with the two proteins forming
245 a heterodimer.

246 Controlled formation of protein condensates can be used by cells for various physiological purposes
247 whereas aggregation of misfolded proteins represents an irreversible loss of protein function (Alberti
248 and Hyman, 2021). To address whether formation of cytosolic Kap95-GFP and Srp1-GFP foci are
249 reversible, we monitored their localization after As(III) exposure during 1 h followed by As(III) washout.
250 NE localization of both proteins slowly recovered after As(III) washout, and this recovery largely
251 coincided with the disappearance of cytosolic Kap95-GFP (Fig. 3C) and Srp1-GFP (Fig. S3B) foci. CHX,
252 added after the washing step, slowed down or prevented the recovery of Kap95-GFP and Srp1-GFP at
253 the NE as well as the disappearance of cytosolic Kap95-GFP and Srp1-GFP foci (Figs. 3C, S3B), indicating
254 that foci reversal and signal recovery at the NE require *de novo* protein synthesis. Thus, formation of
255 Kap95-GFP and Srp1-GFP foci may not be a regulated process that cells use to quickly recover once
256 As(III) stress is relieved.

257 Next, we addressed whether the Kap95-GFP and Srp1-GFP foci represent aggregated forms of these
258 proteins. For this, we isolated total and aggregated proteins by differential centrifugation and

259 separated the proteins in each fraction by SDS-PAGE followed by immunoblotting with an anti-GFP
260 antibody. Both Kap95-GFP and Srp1-GFP were present in the aggregated protein fractions isolated
261 from As(III)-exposed cells while these proteins were largely absent in the aggregated protein fractions
262 of unexposed cells (Fig. 3D). This finding indicates that Kap95 and Srp1 aggregate in the presence of
263 As(III) and that the cytosolic foci likely represent aggregated forms of these proteins. The data also
264 suggest that arsenic-binding to Kap95, in form of MAs(III), is sufficient to induce mislocalization and
265 aggregation of both Srp1 and Kap95 in the heterodimeric α/β complex. Importantly, the karyopherin
266 βs Kap121/Pse1 (Fig. 3D) and Kap123 (Jacobson et al., 2012) also aggregated during As(III) exposure.
267 We conclude that arsenic-binding to nuclear import receptors leads to their relocation from the
268 nuclear envelope and subsequent aggregation in the cytosol.

269

270 **As(III) affects Nup localization, NE morphology, and NPC numbers.**

271 The arsenic-binding Nups identified in this study are located in the outer ring (Nup84, Nup85, Nup120,
272 Nup133, Nup145) and the inner ring (Nup157, Nup170, Nup188, Nup192) of the NPC (Fig. 4A). Nup145
273 is, after proteolytic cleavage, present in the outer ring (Nup145C fragment) and in the NPC core
274 (Nup145N) as one of several so-called FG-Nups that are directly responsible for nucleocytoplasmic
275 transport (Aitchison and Rout, 2012; Wing et al., 2022). Similar to the tested importins, As(III) affected
276 the localization of chromosomally integrated Nup84-GFP and Nup188-GFP. In untreated (control) cells,
277 Nup84-GFP was localized in patches in the NE (Fig. 4B). During As(III) exposure, Nup84-GFP was visible
278 as cytosolic foci and the fluorescence signal appeared to extend from the NE into the cytosol in a
279 substantial fraction of the cells (Figs. 4B, 4C). Likewise, Nup188-GFP was visible in a punctuate pattern
280 in the NE in unexposed cells whereas cytosolic foci and fluorescence signal extensions from the NE into
281 the cytosol were observed in As(III)-exposed cells (Figs. 4B, 4C). CHX did not prevent As(III)-induced
282 Nup84-GFP foci formation (Fig. S4A), suggesting that As(III) affects the localization of the native
283 (folded) form of Nup84. These findings imply that arsenic-binding to Nup84 and Nup188 leads to their
284 mislocalization and that arsenic may cause NE deformations.

285 We next performed immuno- electron microscopy (EM) on untreated and As(III) exposed yeast cells
286 using a primary antibody that detects Nups in conjunction with a secondary 10 nm gold label to
287 simultaneously observe NE morphology, Nup localization, NPC morphology and number, and protein
288 aggregates visible as electron-dense content (EDC) within cells (Panagaki et al., 2021; Schneider et al.,
289 2024). While we did not detect any abnormalities in NPC morphology in As(III)-exposed cells (Fig. 5A),
290 the exposed cells had fewer visible NPCs per cell section compared to unexposed cells (Fig. 5B). The
291 lower number of NPCs is probably not a result of reduced Nup levels during As(III) stress as Nup84-GFP
292 and Nup188-GFP levels remained largely unchanged during exposure (Fig. S4B). Instead, a substantial

293 fraction of Nup immunolabelling was associated with EDCs in As(III)-exposed cells (Fig. 5C), suggesting
294 that Nups may aggregate. These aggregates were not membrane enclosed, but often localized at sites
295 of NE deformations in which the NE extended into the cytoplasm (Fig. 5D, panel I.) or where the inner
296 and outer leaflets were separated with the outer leaflet extending into the cytoplasm (Fig. 5D, panel
297 II.) forming an outer membrane bud. In sum, arsenic-binding to Nups may result in their mislocalization
298 and aggregation, reducing the number of NPCs present on the NE.

299

300 **Nuclear transport is disrupted during long-term As(III) stress.**

301 Having established that importins and Nups mislocalize and aggregate, we next addressed whether
302 nuclear transport is affected in As(III)-exposed cells using established reporters (Barrientos et al., 2023;
303 Rempel et al., 2019). We first monitored the localization of the Srp1/Kap95 substrate GFP-tcNLS (GFP
304 with a tandem classical NLS) under the control of the galactose-inducible *GAL1* promoter. Expression
305 of GFP-tcNLS was induced and localization of GFP-tcNLS determined by calculating the ratio of the
306 fluorescence measured in the nucleus over the cytosol (N/C ratio) in the absence or presence of As(III)
307 (Fig. 6A). Importantly, the N/C ratio significantly decreased in As(III)-exposed cells (Fig. 6B), suggesting
308 that nuclear accumulation of GFP-tcNLS was inhibited. Similarly, the N/C ratios of two other reporters
309 containing NLS sequences recognized respectively by Kap104 (Nab2NLS-GFP) and Kap121/Pse1
310 (Pho4NLS-GFP), also decreased in exposed cells. In contrast, the N/C ratio of GFP without an NLS
311 remained largely unaffected during exposure (Fig. 6B). The total protein levels of Kap95, Srp1 and
312 Kap121/Pse1 were not affected by As(III) (Fig. 3D). Thus, nuclear import of NLS-containing cargos (GFP-
313 tcNLS, Nab2NLS-GFP, Pho4NLS-GFP) is disrupted in As(III) exposed cells, probably due to arsenic-
314 binding to import receptors and Nups.

315 To address if As(III) also affects nuclear export, we monitored the localization of the transcriptional
316 repressor Mig1-GFP, which is nuclear in the presence of glucose but rapidly exits the nucleus via Msn5-
317 dependent export when glucose is replaced by glycerol (DeVit and Johnston, 1999). Note that As(III)
318 directly binds to Msn5 (Fig. 2B). As expected, shifting cells from glucose to glycerol resulted in a
319 substantial drop of nuclear Mig1-GFP within 5 min (Fig. 6C). When cells were preincubated with As(III)
320 for 1 h, glycerol-stimulated nuclear exit of Mig1-GFP was significantly inhibited (Fig. 6C). Thus, As(III)
321 also disrupts nuclear export, possibly as a consequence of arsenic binding to export receptors.

322 Previous work has shown that yeast cells depend on transcriptional regulation of genes required for
323 As(III) tolerance (Wysocki and Tamás, 2010). For instance, the transcription factors Yap1 and Msn2
324 accumulate in the nucleus during As(III) stress where they induce expression of defence genes (Hosiner
325 et al., 2009; Thorsen et al., 2007; Wysocki et al., 2004) while the transcription factor Sfp1 exits the

326 nucleus upon As(III) exposure which results in down-regulation of protein biosynthesis-related genes
327 (Hosiner et al., 2009). Thus, cells rely on functional nucleocytoplasmic transport to mount an
328 appropriate response to arsenic stress. Nuclear accumulation of chromosomally integrated Yap1-GFP
329 and Msn2-GFP, as well as nuclear exit of Sfp1-GFP was efficient within 5-15 min of As(III) exposure (Fig.
330 S6), consistent with their role as As(III)-responsive factors. These data suggest that nuclear protein
331 import and export is not affected during short-term exposure, possibly because the arsenic that enters
332 cells is first recognized by arsenic-specific sensing and signalling systems before sufficient arsenic
333 accumulates to poison cellular functions. Alternatively, these stress-responsive transcription factors
334 might cross the NE through As(III)-insensitive pathways. Collectively, our data suggest that nuclear
335 transport is disrupted during long-term As(III) stress but remains functional in the initial phase of
336 exposure.

337 Our chemical-genetic and genetic interaction data (Fig. S1) suggested that arsenic-binding to proteins
338 mediating nucleocytoplasmic transport causes toxicity. In further support of this notion, cells with
339 weakened (temperature-sensitive) alleles of Kap95 (*kap95*-L63A) and Kap121/Pse1 (*kap121*-Δ34) (Li et
340 al., 2011) were As(III) sensitive (Fig. 7). Thus, disruption of nucleocytoplasmic transport may result in
341 arsenic sensitivity.

342

343

344 **DISCUSSION**

345 This current study strongly implicates nucleocytoplasmic transport as a key target of arsenic toxicity.
346 First, our proteome-wide approach identified 174 arsenic-binding proteins *in vivo*, of which proteins
347 involved in nucleocytoplasmic transport were remarkably enriched. In fact, arsenic bound to most of
348 the importins present in *S. cerevisiae* and we verified arsenic-binding to selected importins, exportins,
349 and Nups. Second, we demonstrated that importins and Nups mislocalized and aggregated, and that
350 the number of NPCs was reduced in As(III) exposed cells. Third, we provided evidence that
351 nucleocytoplasmic transport is impaired during As(III) exposure and that cells with defective nuclear
352 protein transport function are As(III) sensitive. Together, our data are consistent with a model in which
353 arsenic-binding to nuclear transport factors leads to their mislocalization and aggregation, disrupting
354 nucleocytoplasmic transport and causing As(III) sensitivity.

355 Previous *in vivo* proteome-wide studies using the As-biotin probe in various human cell lines typically
356 identified 40-50 candidate arsenic-binding proteins (Dong et al., 2022; Yan et al., 2016; Zhang et al.,
357 2015b; Zhang et al., 2007). Our current study yielded 174 proteins representing, to our knowledge, the
358 largest set of *in vivo* arsenic-binding targets reported to date. Some proteins known to bind to arsenic
359 were absent from our hit list, including the As(III)-sensing transcription factor Yap8 (Kumar et al., 2016).
360 Low-abundance proteins are less represented in our dataset, and some true targets might be missed
361 due to the stringent filtering criteria used. A study that applied As-biotin to a human proteome
362 microarray identified 360 candidate arsenic-binding proteins (Zhang et al., 2015a). It is unclear
363 whether proteins are properly folded on the microarray, which is an important aspect since non-native
364 structures could result in cysteine residues being more easily accessible for arsenic-binding than in
365 folded native proteins. Nevertheless, the authors demonstrated that one of the 360 candidate
366 proteins, hexokinase 2, is a direct target of arsenic inhibition *in vivo* (Zhang et al., 2015a). Collectively,
367 these studies demonstrate the great utility of the As-biotin probe for proteome-wide identification of
368 binding and toxicity targets, and together provide a valuable resource for mechanistic studies of on
369 the toxicity, pathology, and therapeutic effects of arsenicals.

370 While As-biotin is a valuable tool, it cannot discriminate between As(III)- and MAs(III)-binding proteins
371 (Lee and Levin, 2019). By using *mtq2Δ* cells and pretreatments with As(III) and MAs(III) as blocking
372 agents, we identified proteins that bound to either As(III) or MAs(III), or to both arsenicals (Table S2).
373 For example, Kap121/Pse1 and Crm1 bound to both arsenicals whilst Kap95 primarily bound to MAs(III)
374 (Fig. 2C). Interestingly, previous studies indicated that As(III) and MAs(III) can bind to distinct sets of
375 cysteine thiols in target proteins thereby eliciting stress-specific responses (Lee and Levin, 2022). How
376 specific cysteine residues distinguish between As(III) and MAs(III) is not known. While our study
377 suggests that the majority of the 174 arsenic-binding proteins can bind to As(III) as well as MAs(III), the

378 exact form of arsenic, the residues involved, and the physiological consequences of the binding remain
379 to be defined.

380 The observations that As(III)-induced Kap95-GFP and Nup84-GFP foci formation were unaffected in the
381 presence of CHX (Figs. 3B, S4), suggests that arsenic targets the native (folded) form of these proteins
382 promoting their mislocalization and aggregation (Figs. 3, 4, 5). Previously, we showed that As(III)
383 treatment of yeast cells resulted in the formation of Hsp104-GFP foci that could be prevented by CHX
384 (Andersson et al., 2021; Hua et al., 2022; Ibstedt et al., 2014; Jacobson et al., 2012). Based on these
385 and other findings, we concluded that As(III) primarily targets non-native proteins for misfolding and
386 aggregation (Andersson et al., 2021; Hua et al., 2022; Ibstedt et al., 2014; Jacobson et al., 2012). It is
387 important to note that there is a fundamental difference between Hsp104-GFP foci and Kap95-GFP
388 foci that form in As(III)-exposed cells. Hsp104 is a disaggregase that associates with and reactivates
389 aggregated proteins in *S. cerevisiae* (Glover and Lindquist, 1998) and Hsp104-GFP is a well-established
390 marker for cytosolic protein aggregation (Jacobson et al., 2012; Kaganovich et al., 2008; Panagaki et
391 al., 2021). Thus, As(III)-induced Hsp104-GFP foci formation is a consequence of global aggregation of
392 cytosolic proteins to which Hsp104 associates while its own activity is unaffected (Hua et al., 2022;
393 Jacobson et al., 2012). In contrast, Kap95-GFP foci represents aggregated (Fig. 3) and probably
394 unfunctional Kap95 since nuclear import of the Kap95/Srp1 cargo GFP-tcNLS was impaired in As(III)-
395 treated cells (Fig. 6B). Moreover, unlike Hsp104 and it cochaperones, karyopherins are unlikely to
396 recognize misfolded proteins. Thus, native and functional Hsp104-GFP forms foci by associating with
397 non-native proteins while Kap95-GFP (and probably also Nup84-GFP) most likely forms foci because it
398 aggregates. Hence, arsenic can directly modify cysteines in non-native (Hua et al., 2022; Jacobson et
399 al., 2012) as well as native (this work) proteins driving their unfolding and aggregation, with non-native
400 proteins being particularly vulnerable (Tamás et al., 2014; Wysocki et al., 2023). This raises the
401 question if some (or many) of the proteins isolated in the As-biotin experiments are being brought
402 down indirectly in aggregates. However, the As-biotin pull-down experiments would probably not
403 include aggregates because the beads are centrifuged at 1000 x *g*, which is not nearly high enough to
404 sediment aggregates. This is also consistent with the relatively low level of overlap between the
405 proteins identified as arsenic-binding and those identified by sedimentation of As(III)-induced
406 aggregates (Fig. 1F).

407 It has been shown that cytosolic protein aggregates can impair nucleocytoplasmic transport by
408 sequestering nuclear shuttle factors (Woerner et al., 2016). While As(III) induces global aggregation of
409 cytosolic proteins in yeast (Jacobson et al., 2012), our data point to a more direct mechanism where
410 arsenic impairs nucleocytoplasmic transport by binding to nuclear import and export factors. Arsenic
411 may also affect nucleocytoplasmic transport by binding to Nups, which then leads to reduced number

412 of NPCs in the NE (Fig. 5). Additionally, As(III) induces morphological abnormalities of the NE with
413 deformations extending into the cytosol (Fig. 5). Interestingly, genetic perturbations that result in NE
414 aberrations, such as NE protrusions that extend into the cytosol, are linked to loss-of-function
415 mutations of NPC components (Thaller and Lusk, 2018) including several Nups identified in our study
416 (*e.g*. Nup85, Nup188, Nup145). Thus, the observed NE aberration during As(III) stress may be a direct
417 consequence of arsenic-binding to Nups, interfering with their function.

418 Several studies have linked arsenic exposure to an increased prevalence of neurodegenerative
419 disorders such as Alzheimer's and Parkinson's disease (Rahman et al., 2021; Wysocki et al., 2023).
420 These diseases are characterized by the pathological accumulation of protein aggregates (Soto and
421 Pritzkow, 2018), and there is growing evidence that arsenic contributes to these diseases by impairing
422 protein folding in cells (Wysocki et al., 2023). Interestingly, mislocalization of nucleocytoplasmic
423 transport factors, such as Nups and importins, and the disruption of nucleocytoplasmic transport have
424 been implicated in the pathology of neurodegenerative disorders (Hutten and Dormann, 2020; Kim
425 and Taylor, 2017). Thus, the observed impairment of nucleocytoplasmic transport by arsenic, via direct
426 binding, mislocalization, and aggregation of individual nuclear transport factors described in this
427 current study, may be an additional mechanism by which this metalloid contributes to pathology.

428 In conclusion, our study provides novel insights into the molecular mechanisms by which arsenic
429 disrupts cellular function, specifically its impact on nucleocytoplasmic transport. These findings have
430 broad implications for understanding how environmental poisons affect cells and organisms and may
431 serve as a basis for future research on the toxic and therapeutic effects of arsenicals.

432

433

434

435

436 **MATERIALS AND METHODS**

437 **Yeast strains, plasmids, and culturing conditions**. All yeast strains and plasmids used in this work are
438 listed in Table S3. The *S. cerevisiae* strains are based on BY4741 (Brachmann et al., 1998), the deletion
439 collection (Giaever et al., 2002), the collection of temperature-sensitive mutants of essential yeast
440 genes (Li et al., 2011), and the GFP collection (Huh et al., 2003). The strains harbouring nuclear
441 transport reporters have been described previously (Rempel et al., 2019).

442 Plasmids containing HA-tagged versions of Kap123, Sxm1, Nup84, and Nup188 were constructed via
443 Gateway Recombination Cloning (Thermo Fisher Scientific, Waltham, MA, USA) in accordance with the
444 manufacturer's instructions. Gene sequences were amplified by PCR using genomic DNA as template,
445 inserted into the donor plasmid pDONR221 (Thermo Fisher Scientific, Waltham, MA, USA) and then
446 into the destination vector pAG426GPD-ccdB-HA (Addgene plasmid #14252;
447 http://n2t.net/addgene:14252) (Alberti et al., 2007). All plasmids were verified by sequencing.

448 Cells were routinely grown at 30°C in minimal YNB (yeast nitrogen base) medium with 2% glucose as
449 carbon source. Cells containing nuclear transport reporters were grown with 2% raffinose as carbon
450 source and protein expression was induced with 0.5% galactose for 4 h. For growth assays on plates,
451 cells were grown until log phase, the optical density (OD) at 600 nm adjusted to equal for all cultures,
452 diluted in 10-fold steps, plated using a sterilized stamp, and incubated for 2–3 days at 30°C. Where
453 indicated, the following chemicals were added: sodium arsenite ($NaAsO_2$, S7400), cycloheximide
454 (C7698) (both from Sigma-Aldrich, St. Louis, MO, USA), biotinyl p-aminophenyl arsenic acid (As-biotin,
455 B394970; Toronto Research Chemicals, North York, Canada), and monomethylarsonous acid (CH_5AsO_2,
456 M565100; LGC Standards, Wesel, Germany).

457

458 **Arsenic-binding assays.** Proteome-wide identification of arsenic-binding proteins was performed with
459 *mtq2Δ* cells grown to early log phase in YNB medium. For the last hour, the medium was switched to
460 YEPD (Yeast Extract Peptone Dextrose) with 2% glucose and split into control and treatment cultures.
461 The cultures were pretreated for 10 min with either As(III) or MAs(III) as blocking agents, followed by
462 10 min incubation with As-biotin at 30°C. The cultures were collected, pelleted, and frozen at -80°C or
463 lysed directly. Cell lysis was performed by bead beating (1 min, 4°C) in IP buffer (1x TNT buffer (50 mM
464 Tris-HCl, pH 7.5, 150 mM NaCl, 0.5% Triton, pH 7-7.5)), 1x protease inhibitor (Complete mini, EDTA-
465 free; Roche), 1x phosphatase inhibitor (PhosSTOP Easypack; Roche), and 1 mM phenylmethylsulfonyl
466 fluoride (PMSF). Streptavidin agarose beads (ThermoFisher, 20353) were prepared by a 1x TNT buffer
467 wash and aliquoted to all lysates. After a 1 h incubation (4°C, rotating), pull-down was performed by
468 centrifugation (1000x *g*, 1 min) and washing three times in 1x TNT. Proteins present in the pull-down

469 were separated by SDS-PAGE electrophoresis followed by identification using microcapillary liquid
470 chromatograph-tandem mass spectrometry (LC/MS/MS) at the Taplin Mass Spectrometry Facility at
471 Harvard Medical School. To validate arsenic-binding to selected proteins, we used wild type cells
472 carrying plasmids with HA-tagged versions of the corresponding genes or cells that harboured GFP-
473 tagged versions of the genes in their genomes. After As-biotin pull-down and SDS-PAGE as described
474 above, the proteins were visualized by Western blotting using anti-GFP rabbit IgG (1:8000, A11122;
475 Invitrogen, Waltham, MA, USA) or anti-HA mouse IgG (1:1000, sc-7392; Santa Cruz Biotechnologies,
476 Dallas, TX, USA) primary antibodies, and anti-rabbit IgG (1:3000, 84564) and anti-mouse IgG (1 : 5000,
477 84545) secondary antibodies (both from Invitrogen (Waltham, MA, USA)). A more extensive
478 description of the Western blot protocol is provided in the section 'Protein aggregate isolation and
479 Western blotting' below.

480

481 **Bioinformatics and protein structure analyses**. Negative genetic interactors (including negative
482 genetic, synthetic growth defect, synthetic lethality) of selected arsenic-binding hits were retrieved
483 from the *Saccharomyces* genome database (SGD) (Wong et al., 2023) and compared to a compendium
484 of 712 As(III) sensitive *S. cerevisiae* mutants that contains the genes identified at least once in four
485 previous genome-wide phenotypic screens (Haugen et al., 2004; Pan et al., 2010; Thorsen et al., 2009;
486 Zhou et al., 2009). The significance of the overlaps between datasets was calculated by the hyper-
487 geometric test. All datasets used for comparisons are listed in Table S4. For protein structure analyses,
488 protein sequences were retrieved from SGD. PDB files were retrieved from the AlphaFold protein
489 structure database (Jumper et al., 2021) and visualized using UCSF ChimeraX version: 1.6.1 (Goddard
490 et al., 2018).

491

492 **Fluorescence microscopy and image analyses.** Cells expressing GFP-tagged proteins were grown until
493 mid-log phase and either left untreated or exposed to As(III) and/or 0.2 mg/ml CHX added to the
494 culture at the same time as the As(III). To induce nuclear export of Mig1-GFP, cells were first grown in
495 glucose-containing medium and then shifted to medium containing 2% glycerol. Where indicated, cells
496 were pretreated with 1.5 mM As(III) for 1 h. All samples were fixed in 3.7% formaldehyde (RT, 30 min)
497 followed by two washes in 1x PBS. Nuclear staining was done by incubating fixed cells in ethanol (RT,
498 40 min), washing in 1x PBS, and resuspending in 4',6-diamidino-2-phenylindole (DAPI) solution (D1306;
499 Thermo Fisher Scientific). Fluorescent signals were detected using a Zeiss Axiovert 200 M (Carl Zeiss
500 Microscopy, München, Germany) fluorescence microscope equipped with Plan-Apochromat 1.40
501 objectives and appropriate fluorescence light filter sets. Images were taken with a digital camera

502 (AxioCamMR3). The ZEISS ZEN PRO software (Carl Zeiss Microscopy) was used to capture the images
503 and the ImageJ-Fiji software (Schindelin et al., 2012) for quantifications.

504 The steady-state localization of nuclear transport reporters (GFP-tcNLS, Nab2NLS-GFP, Pho4NLS-GFP,
505 GFP) was determined largely as described previously (Barrientos et al., 2023; Rempel et al., 2019). Cells
506 were grown to mid-log phase in YNB medium containing 2% raffinose and then expression of the
507 reporters was induced by the addition of 0.5% galactose for 4 h followed by the addition of 1.5 mM
508 As(III) for 1 h. N/C ratios were quantified by measuring the mean fluorescence intensity in the nucleus
509 and in the cytosol. The nucleus was outlined along the NE using Nup49-mCherry. Care was taken to
510 exclude the vacuole when choosing a field in the cytosol. All measured values were corrected for
511 background fluorescence and the ratio of nuclear versus cytosolic signal (N/C ratio) was calculated for
512 three replicates and averaged.

513

514 **Protein aggregate isolation and Western blotting.** Insoluble protein aggregates were isolated as
515 described previously (Hua et al., 2022; Weids and Grant, 2014). Cells were grown to mid-log phase,
516 unexposed or exposed to 1.5 mM As(III), collected by centrifugation, resuspended in lysis buffer (50
517 mM potassium phosphate buffer pH 7, 1 mM EDTA, 5% glycerol, 1 mM PMSF, EDTA-free protease
518 inhibitor cocktail from Roche Diagnostics, Basel, Switzerland), and lysed with 2.5 mg/ml lyticase
519 (Sigma-Aldrich: 30 min, 30°C). Cells were disrupted using sonication on ice (Sonifier 150, Branson
520 Ultrasonics, Danbury, CT, USA; 8x 5 s pulses, 50% amplitude) and the total lysates collected by
521 centrifugation. Protein concentrations in the lysates were adjusted to equal for all samples. Aggregated
522 proteins were isolated by centrifugation of the protein lysates, resuspended in lysis buffer containing
523 20% NP40 twice, followed by washing and resuspension of the pellet in lysis buffer. The final
524 resuspension was aided by sonication (2x5 sec, 50% amplitude on ice). 5X SDS loading buffer (4% SDS,
525 250 mM Tris Buffer pH 6.8, 16% β-mercaptoethanol, 30% glycerol, bromophenol blue) was added to
526 all samples followed by boiling for 5 min at 95°C. Proteins were separated on a Criterion 4-20% stain
527 free precast gel (Bio-Rad Laboratories, Hercules, CA, USA) and visualized using a ChemiDoc XRS+
528 system with UV-activation (Bio-Rad). For Western blot analysis, proteins were transferred to a PVDF
529 membrane using TransBlot Turbo transfer system (semi-dry transfer, Bio-Rad). Membranes were
530 blocked with 5% bovine serum albumin (BSA) in Tris-buffered saline (TBS) containing 0.05% Tween 20
531 (TBS-T) for 1 h at RT followed by over-night incubation at 4°C with an anti-GFP antibody (1:8000,
532 A11122; Invitrogen, Waltham, MA, USA). Membranes were washed 3X with TBS-T, incubated for 2 h
533 with anti-rabbit-IgG secondary antibody (1:5000, 84546; Invitrogen, Waltham, MA, USA) and washed
534 with TBS-T followed by signal detection using the ChemiDoc system.

535

536 **Immuno-electron microscopy.** Immuno-EM was performed largely as described previously (Panagaki
537 et al., 2021). Cells were grown to early log phase and either left untreated or exposed to 1.5 mM As(III)
538 for 1 h. Samples were high-pressure frozen (Wohlwend HPF Compact 3, Sennwald, Switzerland)
539 followed by freeze substitution in 2% uranyl acetate (UA) dissolved in acetone, and embedded into
540 HM20 lowicryl resin (Polysciences) that was UV polymerised at -50°C. The resin was sectioned in 70
541 nm thin sections and placed on mesh grids. The sections were fixed in 1% paraformaldehyde in PBS for
542 10 min and blocked with 0.1% fish skin gelatine and 0.8% BSA in PBS for 1 h. For detection of Nups,
543 samples were incubated for 2 h with 1:120 dilution of the mouse monoclonal anti-NPC antibody
544 Mab414 (Abcam ab24609) at 4°C, followed by incubations at room temperature with 1:150 dilution of
545 rabbit anti-mouse immunoglobulin (Agilent/Dako, E0433) for 1 h and with 1:70 diluted 10 nm gold-
546 conjugated protein A antibody (CMC UMC Utrecht, The Netherlands) for 30 min. Glutaraldehyde (2.5%)
547 was applied to sections for 1 h, followed by contrast staining in 2% UA for 5 min and 1 min in Reynold's
548 lead citrate (Reynolds, 1963). Three washing steps (20 min, PBS) were carried out after incubations
549 with each antibody. Images were acquired at 120 kV on a Tecnai T12 transmission electron microscope
550 equipped with a Ceta CMOS 16M camera (Thermofischer scientific, Eindhoven, the Netherlands).
551 Quantifications were made using IMOD (Kremer et al., 1996) and statistics with GraphPad Prism 10.

552

553 **Acknowledgements**

554 We thank Liesbeth M. Veenhoff (University of Groningen) for providing yeast strains. pAG426GPD-
555 ccdB-HA was a gift from Susan Lindquist (Addgene plasmid #14252; http://n2t.net/addgene:14252;
556 RRID:Addgene_14252).

557

558 **Funding**

559 This work was supported by grants from the National Institutes of Health (grant numbers
560 R01GM138413 and R01GM48533) to D.E.L., Cancerfonden (grant number 211-865) and the Swedish
561 Research Council (grant number 2019-4004) to J.L.H., the foundations Bengt Lundqvist minne och Sven
562 och Dagmar Saléns Stiftelse to E.L., and the Swedish Research Council (grant number 2018-03577) and
563 Olle Engkvists Stiftelse (grant number 216-0452) to M.J.T.

564

565 **Author contributions**

566 D.E.L., J.L.H., and M.J.T. - conceptualization;

E.L., J.L., J.M., K.K., N.K., C.G., R.M. - investigation;

E.L., J.L., J.M., K.K., N.K., C.G., R.M., J.L.H., D.E.L., M.J.T. - formal analysis;

E.L. and M.J.T. – writing the original draft;

E.L., J.L., J.M., K.K., N.K., C.G., R.M., J.L.H., D.E.L., M.J.T. - review & editing;

E.L., D.E.L., J.L.H., and M.J.T. - funding acquisition.

Conflict of interest

The authors declare no conflicts of interest.

576 **FIGURE LEGENDS**

577 **Figure 1. Proteome-wide screen identifies arsenic-binding proteins and toxicity targets.**

578 **1A**. Workflow. Yeast cells (*mtq2Δ*) were incubated with 50 µM As-biotin without or with a 10 min
579 pretreatment with 1 mM As(III) or 500 µM MAs(III) as blocking agents. After cell disruption and protein
580 pull-down using streptavidin beads, the proteins present in the pull-down were identified using LC-
581 MS/MS. The data was filtered using the following stringent criteria: (1) no peptide present in the
582 control, (2) ≥5 unique peptides identified per protein after As-biotin pull-down, and (3) ≥2-fold
583 reduction of signal/peptide intensity when competitor As(III) or MAs(III) was present during pull-down.
584 A total of 174 candidate arsenic-binding proteins were identified.

585 **1B**. Cysteine content and motifs in arsenic-binding proteins versus a proteome of around 5800 proteins
586 (Ho et al., 2018). x represents any amino acid present between the cysteine residues in a motif.
587 Significance was calculated by the hyper-geometric test, and *P*-values are according to: * < 0.05, ** <
588 0.01, and *** < 0.001.

589 **1C-F**. Venn diagrams show the overlap between arsenic-binding proteins and: **C)** proteins containing
590 surface-exposed cysteine residues (Marino et al., 2010), **D)** As(III)-sensitive heterozygous diploid
591 knockout mutants (Pan et al., 2010), **E)** essential proteins in *S. cerevisiae* (extracted from SGD (Wong
592 et al., 2023)), and **F)** proteins aggregating during As(III) exposure (Ibstedt et al., 2014; Jacobson et al.,
593 2012). The significance of the overlaps between the datasets was calculated by the hyper-geometric
594 test and the corresponding *P*-values are indicated.

595

596 **Figure 2. Arsenic binds to proteins involved in nucleocytoplasmic transport.**

597 **2A**. Bar plots of overrepresented GO-terms in the arsenic-binding protein set using Metascape (Zhou
598 et al., 2019).

599 **2B**. Cells expressing HA-tagged or GFP-tagged versions of Sxm1, Kap123, Msn5, Nup84, Nup188 and
600 Srp1 were incubated with 50 µM As-biotin followed by cell disruption and protein pull-down using
601 streptavidin beads. The proteins were detected by Western blotting using anti-HA and anti-GFP
602 antibodies. Cells were pretreated with 1 mM As(III) as blocking agent as indicated. The loading control
603 (Input) represents the total lysate. The blots shown are representative of at least two biological
604 repeats.

605 **2C**. As-biotin pulldown assays were performed as in 2B using cells expressing GFP-tagged Kap95,
606 Kap121/Pse1 and Crm1. The proteins were detected by Western blotting using an anti-GFP antibody.

607 Cels were pretreated with 1 mM As(III) or 1 mM MAs(III) as blocking agents as indicated. The blots
608 shown are representative of at least two biological repeats.

609 **2D**. Cysteine content and motifs in the listed proteins. x represents any amino acid present between
610 the cysteine residues in a motif.

611

612 **Figure 3. Importins mislocalize and aggregate in As(III)-exposed cells.**

613 **3A**. Localization of GFP-tagged Kap95 and Srp1. In unexposed (control) cells the proteins are located
614 around the NE (white arrowheads). After As(III) exposure (1.5 mM) for 1 h, the proteins are found in
615 distinct foci dispersed throughout the cytosol (red arrowheads). Images shown are representative of
616 three biological repeats of 100 cells each.

617 **3B**. Quantification of Kap95-GFP NE localization (left panel) and cytosolic foci formation (right panel)
618 in the absence and presence of 1.5 mM As(III) and/or 0.2 mg/ml cycloheximide (CHX). Kap95–GFP
619 distribution was scored by fluorescence microscopy and quantified by visual inspection. The bars
620 represent the mean ± standard deviation (SD) of three independent biological repeats of a total of 300
621 cells. Significance was calculated using un-paired two-tailed student's t-test with either the untreated
622 control (for just As(III) exposure) or CHX (for CHX+As(III)-treated cells) as the comparison. *P*-values are
623 according to: ** > 0.01, *** > 0.001.

624 **3C**. Cells were exposed to 1.5 mM As(III) for 1 h, then washed twice and resuspended in medium
625 without As(III) in the presence or absence of 0.2 mg/ml CHX. Kap95–GFP distribution was scored and
626 quantified as in 3B. The bars represent the mean ± SD of three independent biological repeats of a
627 total of 300 cells. Significance was calculated using un-paired two-tailed student's t-test of three
628 independent biological replicates, with 1 h As(III) exposed cells as the control. *P*-values are according
629 to: * > 0.05, ** > 0.01, *** > 0.001.

630 **3D**. Kap95, Srp1, and Kap121/Pse1 aggregate in the presence of As(III). Cells expressing GFP-tagged
631 proteins were left untreated (control) or exposed to 1.5 mM As(III), lysed, and the total and aggregated
632 protein fractions were isolated followed by Western blot analysis using an anti-GFP antibody. The blots
633 shown are representative of at least two biological repeats.

634

635 **Figure 4. As(III) affects Nup localization in cells.**

636 **4A.** Illustration of the yeast NPC with the arsenic-binding Nups and their respective subcomplex.

637 **4B**. Localization of GFP-tagged Nup84 and Nup188. In unexposed (control) cells the proteins are
638 located around the NE (white arrowheads). After 1 h of As(III) exposure (1.5 mM), the proteins are

639 visible as cytosolic foci, often with the fluorescence signal extending from the NE into the cytosol (red
640 arrowheads). The images shown are representative of three biological repeats of 100 cells each.

641 **4C**. Nup84–GFP and Nup188-GFP distribution was scored by fluorescence microscopy and quantified
642 as in Figure 3B. The bars represent the mean ± SD of three independent biological repeats of a total of
643 300 cells. *P*-values are according to * > 0.05, ** > 0.01, *** > 0.001.

644

645 **Figure 5. As(III) affects NE morphology and NPC numbers.**

646 **5A**. Representative electron micrographs of yeast cells before and after exposure to 1.5 mM As(III) for
647 1 h. The boxes correspond to areas showing NPCs that appear as holes in the NE bilayer. Nup
648 localization was addressed with a gold-labelled anti-Nup antibody (Mab414). Protein aggregates
649 appear as electron dense content (EDC) both in nucleus and in areas that are free of ribosomes in the
650 cytosol (Panagaki et al., 2021). A model is drawn below each micrograph to visualize the locations of
651 gold particles and EDCs.

652 **5B-C**. Quantification of the number of NPCs per cell section (in **C**) and of the fraction of Nups associated
653 with EDCs/protein aggregates (in **D**) in unexposed (control) and As(III)-exposed cells. Nups were
654 detected using a gold-labelled anti-Nup antibody (Mab414).

655 **5D**. Representative electron micrographs of yeast nuclei of cells exposed to 1.5 mM As(III) for 1 h
656 showing NE deformations (arrowheads) in which the NE extends into the cytoplasm (panel I.) and
657 where the inner and outer leaflets are separated with the outer leaflet extending into the cytoplasm
658 (panel II.) forming an outer membrane bud (OM bud), often near EDCs/protein aggregates. A model
659 is drawn to the right of each micrograph to visualize the two types of NE deformation.

660 **5E**. Quantification of the fraction of NE deformations and outer membrane buds (OM bud) per cell
661 section in unexposed (control) and As(III)-exposed cells.

662 The number of cell sections assessed per condition was 62 for control and 74 for As(III) exposed cells.
663 Significance was calculated using an unpaired t-test, and the *P*-values are according to: **> 0.01, ***>
664 0.001, and **** > 0.0001. N, nucleus; EDC, electron dense content, OM bud, outer membrane bud.

665

666 **Figure 6. Nuclear transport is disrupted during As(III) stress.**

667 **6A**. Model of the assay. Yeast cells expressing GFP-tagged nuclear transport reporters were either left
668 untreated or exposed to As(III). N/C ratios were calculated by measuring the mean fluorescence
669 intensities in the nucleus (N) and the cytosol (C).

670 **6B**. Nuclear protein import is inhibited by As(III). N/C ratios were determined in the absence (control)
671 and presence of 1.5 mM As(III) for GFP-tcNLS (recognized by Kap95/Srp1), Nab2NLS-GFP (recognized
672 by Kap104) and Pho4NLS-GFP (recognized by Kap121/Pse1). GFP without sorting sequence was
673 included as a control. The graphs show the mean of three biological replicates of around 100 cells per
674 condition measured.

675 **6C**. Nuclear export is inhibited by As(III). Mig1-GFP localization was determined in the presence of
676 glucose and 5 min after a shift to glycerol. Where indicated, cells were preincubated with 1.5 mM As(III)
677 for 1 h before the shift to glycerol. Mig1-GFP distribution was scored by fluorescence microscopy and
678 quantified as in Figure 3B. The bars represent the mean ± SD of three independent biological repeats
679 of a total of 300 cells. Significance for 6B-C was calculated using an unpaired t-test, and *P*-values are
680 according to: *> 0.05, **> 0.01, ***> 0.001, and **** > 0.0001.

681

682 **Figure 7. Cells defective in nuclear transport function are As(III) sensitive.**
683 Yeast cells that carry a weakened (temperature-sensitive) allele of Kap95 (*kap95-L63A*) or Kap121/Pse1
684 (*kap121-Δ34*) were grown to log phase, adjusted to the same OD, serially diluted, and plated onto YNB
685 medium with 2% glucose as carbon source and the indicated As(III) concentrations. Plates were
686 incubated at 30°C for 3 days. Images shown are representative of three biological replicates.

687

688

689 **SUPPLEMENTARY MATERIAL**

690 **Table S1.** All proteins detected by LC/MS/MS (data file).

691 **Table S2.** List of 174 candidate arsenic-binding proteins.

692 **Table S3**. List of strains and plasmids used.

693 **Table S4**. Datasets used for comparisons.

694

695 **Figure S1**. Integration of chemical-genetic and genetic interaction data to identify *bona fide* arsenic
696 toxicity targets. Negative genetic interactors (including negative genetic, synthetic growth defect,
697 synthetic lethality) of selected arsenic-binding hits were retrieved from SGD (Wong et al., 2023) and
698 compared to a compendium of 712 As(III) sensitive *S. cerevisiae* mutants that contains the genes
699 identified at least once in four genome-wide phenotypic screens (Haugen et al., 2004; Pan et al., 2010;
700 Thorsen et al., 2009; Zhou et al., 2009). The significance of the overlaps between the datasets (negative
701 genetic interactor sets and As(III) sensitive set) was calculated by the hyper-geometric test and the
702 corresponding *P*-values are indicated.

703

704 **Figure S2.** AlphaFold structure predictions and cysteine mapping for Srp1, Kap95, Kap121/Pse1, Crm1,
705 Kap123, Sxm1/Kap108, Msn5, Nup84, and Nup188. Distances between pairs of adjacent or proximal
706 cysteines are indicated. The structure predictions are based on experimental crystal structure data for
707 all proteins except for Kap123, Kap108/Sxm1 and Msn5.

708

709 **Figure S3. Mislocalization of Srp1 in As(III)-exposed cells.**

710 **S3A**. Quantification of Srp1-GFP nuclear envelope (NE) localization (left panel) and foci formation (right
711 panel) in the presence and absence of 1.5 mM As(III) and/or 0.2 mg/ml cycloheximide (CHX). Srp1–GFP
712 distribution was scored by fluorescence microscopy and quantified by visual inspection. The bars
713 represent the mean ± SD of three independent biological repeats of a total of 300 cells. Significance
714 was calculated using un-paired two-tailed student's t-test with either the untreated control (for just
715 As(III)-exposure) or CHX (for CHX+As(III) treated cells) as the comparison, and *P*-values are according
716 to: ** > 0.01, *** > 0.001.

717 **S3B**. Cells were exposed to 1.5 mM As(III) for 1 h, then washed twice and resuspended in medium
718 without As(III) in the presence or absence of 0.2 mg/ml CHX. Srp1–GFP distribution was scored by
719 fluorescence microscopy and quantified as in S3A. Significance was calculated using un-paired two-

720 tailed student's t-test of three independent biological replicates, with 1 h As(III)-exposed cells as the
721 control sample. *P*-values according to * > 0.05, ** > 0.01, *** > 0.001.

722

723 **Figure S4. Nup localization and levels during As(III) stress.**

724 **S4A.** Cycloheximide (CHX) does not prevent Nup84-GFP mislocalization in As(III)-stressed cells.
725 Quantification of Nup84-GFP foci formation in the presence or absence of 1.5 mM As(III) and 0.2 mg/ml
726 CHX. Foci formation was detected with fluorescence microscopy and quantified by visual inspection.
727 The bars represent the mean ± SD of three independent biological repeats of a total of 300 cells.
728 Significance was calculated using un-paired two-tailed student's t-test with CHX-treated cells as the
729 comparison, and P-values are according to: ** > 0.01, *** > 0.001.

730 **S4B.** Nup84-GFP and Nup188-GFP protein levels are largely unaffected by As(III). Western blot of the
731 total lysate from cells expressing Nup84-GFP or Nup188-GFP in the absence (control) and presence of
732 As(III). The lower panel shows the corresponding SDS-PAGE gels as loading controls. The images shown
733 are representative of at least two biological repeats.

734

735 **Figure S5. Nuclear transport is unaffected during short-term As(III) exposure.**

736 Cells expressing GFP-tagged versions of the transcription factors Yap1, Msn2, and Sfp1 were either left
737 untreated (control) or exposed to the indicated concentrations of As(III), and their localization
738 determined by fluorescence microscopy. Quantification was done by visual inspection and the bars
739 represent the mean ± SD of three independent biological repeats of a total of 300 cells. Significance
740 was calculated using un-paired two-tailed student's t-test with the untreated control at the respective
741 time point as the comparison, and *P*-values are according to: *> 0.05, ** > 0.01, *** > 0.001.

742

743

744 **REFERENCES**

745 Aitchison, J.D., and M.P. Rout. 2012. The yeast nuclear pore complex and transport through it.
746 *Genetics*. 190:855-883.
747 Alberti, S., A.D. Gitler, and S. Lindquist. 2007. A suite of Gateway cloning vectors for high-throughput
748 genetic analysis in *Saccharomyces cerevisiae*. *Yeast*. 24:913-919.
749 Alberti, S., and A.A. Hyman. 2021. Biomolecular condensates at the nexus of cellular stress, protein
750 aggregation disease and ageing. *Nat Rev Mol Cell Biol*. 22:196-213.
751 Andersson, S., A. Romero, J.I. Rodrigues, S. Hua, X. Hao, T. Jacobson, V. Karl, N. Becker, A. Ashouri, S.
752 Rauch, T. Nyström, B. Liu, and M.J. Tamás. 2021. Genome-wide imaging screen uncovers
753 molecular determinants of arsenite-induced protein aggregation and toxicity. *J Cell Sci*.
754 134:jcs258338.
755 Barrientos, E.C.R., T.A. Otto, S.N. Mouton, A. Steen, and L.M. Veenhoff. 2023. A survey of the specificity
756 and mechanism of 1,6 hexanediol-induced disruption of nuclear transport. *Nucleus*.
757 14:2240139.
758 Bergquist, E.R., R.J. Fischer, K.D. Sugden, and B.D. Martin. 2009. Inhibition by methylated organo-
759 arsenicals of the respiratory 2-oxo-acid dehydrogenases. *J Organomet Chem*. 694:973-980.
760 Brachmann, C.B., A. Davies, G.J. Cost, E. Caputo, J. Li, P. Hieter, and J.D. Boeke. 1998. Designer deletion
761 strains derived from *Saccharomyces cerevisiae* S288C: a useful set of strains and plasmids for
762 PCR-mediated gene disruption and other applications. *Yeast*. 14:115-132.
763 Chen, Q.Y., and M. Costa. 2021. Arsenic: A Global Environmental Challenge. *Annu Rev Pharmacol*.
764 61:47-63.
765 Chen, Q.Y., T. DesMarais, and M. Costa. 2019. Metals and Mechanisms of Carcinogenesis. *Annu Rev*
766 *Pharmacol Toxicol*. 59:537-554.
767 DeVit, M.J., and M. Johnston. 1999. The nuclear exportin Msn5 is required for nuclear export of the
768 Mig1 glucose repressor of *Saccharomyces cerevisiae*. *Curr Biol*. 9:1231-1241.
769 Dong, X., P. Wang, and Y. Wang. 2022. Chemoproteomic Approach for the Quantitative Identification
770 of Arsenic-Binding Proteins. *Chem Res Toxicol*. 35:2145-2151.
771 Giaever, G., A.M. Chu, L. Ni, C. Connelly, L. Riles, S. Veronneau, S. Dow, A. Lucau-Danila, K. Anderson,
772 B. Andre, A.P. Arkin, A. Astromoff, M. El-Bakkoury, R. Bangham, R. Benito, S. Brachat, S.
773 Campanaro, M. Curtiss, K. Davis, A. Deutschbauer, K.D. Entian, P. Flaherty, F. Foury, D.J.
774 Garfinkel, M. Gerstein, D. Gotte, U. Guldener, J.H. Hegemann, S. Hempel, Z. Herman, D.F.
775 Jaramillo, D.E. Kelly, S.L. Kelly, P. Kotter, D. LaBonte, D.C. Lamb, N. Lan, H. Liang, H. Liao, L. Liu,
776 C. Luo, M. Lussier, R. Mao, P. Menard, S.L. Ooi, J.L. Revuelta, C.J. Roberts, M. Rose, P. Ross-
777 Macdonald, B. Scherens, G. Schimmack, B. Shafer, D.D. Shoemaker, S. Sookhai-Mahadeo, R.K.
778 Storms, J.N. Strathern, G. Valle, M. Voet, G. Volckaert, C.Y. Wang, T.R. Ward, J. Wilhelmy, E.A.
779 Winzeler, Y. Yang, G. Yen, E. Youngman, K. Yu, H. Bussey, J.D. Boeke, M. Snyder, P. Philippsen,
780 R.W. Davis, and M. Johnston. 2002. Functional profiling of the *Saccharomyces cerevisiae*
781 genome. *Nature*. 418:387-391.
782 Giaever, G., D.D. Shoemaker, T.W. Jones, H. Liang, E.A. Winzeler, A. Astromoff, and R.W. Davis. 1999.
783 Genomic profiling of drug sensitivities via induced haploinsufficiency. *Nat Genet*. 21:278-283.
784 Glover, J.R., and S. Lindquist. 1998. Hsp104, Hsp70, and Hsp40: a novel chaperone system that rescues
785 previously aggregated proteins. *Cell*. 94:73-82.
786 Goddard, T.D., C.C. Huang, E.C. Meng, E.F. Pettersen, G.S. Couch, J.H. Morris, and T.E. Ferrin. 2018.
787 UCSF ChimeraX: Meeting modern challenges in visualization and analysis. *Protein Sci*. 27:14-
788 25.
789 Guerra-Moreno, A., M.A. Prado, J. Ang, H.M. Schnell, Y. Micoogullari, J.A. Paulo, D. Finley, S.P. Gygi,
790 and J. Hanna. 2019. Thiol-based direct threat sensing by the stress-activated protein kinase
791 Hog1. *Sci Signal*. 12:eaaw4956.
792 Haugen, A.C., R. Kelley, J.B. Collins, C.J. Tucker, C. Deng, C.A. Afshari, J.M. Brown, T. Ideker, and B. Van
793 Houten. 2004. Integrating phenotypic and expression profiles to map arsenic-response
794 networks. *Genome Biol*. 5:R95.

795 Ho, B., A. Baryshnikova, and G.W. Brown. 2018. Unification of Protein Abundance Datasets Yields a
796 Quantitative *Saccharomyces cerevisiae* Proteome. *Cell Syst*. 6:192-205 e193.
797 Hosiner, D., H. Lempiainen, W. Reiter, J. Urban, R. Loewith, G. Ammerer, R. Schweyen, D. Shore, and
798 C. Schuller. 2009. Arsenic toxicity to *Saccharomyces cerevisiae* is a consequence of inhibition
799 of the TORC1 kinase combined with a chronic stress response. *Mol Biol Cell*. 20:1048-1057.
800 Hua, S., A. Klosowska, J.I. Rodrigues, G. Petelski, L.A. Esquembre, E. Lorentzon, L.F. Olsen, K. Liberek,
801 and M.J. Tamás. 2022. Differential contributions of the proteasome, autophagy, and
802 chaperones to the clearance of arsenite-induced protein aggregates in yeast. *J Biol Chem*.
803 298:102680.
804 Huh, W.K., J.V. Falvo, L.C. Gerke, A.S. Carroll, R.W. Howson, J.S. Weissman, and E.K. O'Shea. 2003.
805 Global analysis of protein localization in budding yeast. *Nature*. 425:686-691.
806 Hutten, S., and D. Dormann. 2020. Nucleocytoplasmic transport defects in neurodegeneration - Cause
807 or consequence? *Semin Cell Dev Biol*. 99:151-162.
808 Ibstedt, S., T.C. Sideri, C.M. Grant, and M.J. Tamás. 2014. Global analysis of protein aggregation in yeast
809 during physiological conditions and arsenite stress. *Biology open*. 3:913-923.
810 Jacobson, T., C. Navarrete, S.K. Sharma, T.C. Sideri, S. Ibstedt, S. Priya, C.M. Grant, P. Christen, P.
811 Goloubinoff, and M.J. Tamás. 2012. Arsenite interferes with protein folding and triggers
812 formation of protein aggregates in yeast. *J Cell Sci*. 125:5073-5083.
813 Jumper, J., R. Evans, A. Pritzel, T. Green, M. Figurnov, O. Ronneberger, K. Tunyasuvunakool, R. Bates,
814 A. Zidek, A. Potapenko, A. Bridgland, C. Meyer, S.A.A. Kohl, A.J. Ballard, A. Cowie, B. Romera-
815 Paredes, S. Nikolov, R. Jain, J. Adler, T. Back, S. Petersen, D. Reiman, E. Clancy, M. Zielinski, M.
816 Steinegger, M. Pacholska, T. Berghammer, S. Bodenstein, D. Silver, O. Vinyals, A.W. Senior, K.
817 Kavukcuoglu, P. Kohli, and D. Hassabis. 2021. Highly accurate protein structure prediction with
818 AlphaFold. *Nature*. 596:583-589.
819 Kaganovich, D., R. Kopito, and J. Frydman. 2008. Misfolded proteins partition between two distinct
820 quality control compartments. *Nature*. 454:1088-1095.
821 Kim, H.J., and J.P. Taylor. 2017. Lost in Transportation: Nucleocytoplasmic Transport Defects in ALS and
822 Other Neurodegenerative Diseases. *Neuron*. 96:285-297.
823 Kitchin, K.T., and K. Wallace. 2008. The role of protein binding of trivalent arsenicals in arsenic
824 carcinogenesis and toxicity. *J Inorg Biochem*. 102:532-539.
825 Kremer, J.R., D.N. Mastronarde, and J.R. McIntosh. 1996. Computer visualization of three-dimensional
826 image data using IMOD. *J Struct Biol*. 116:71-76.
827 Kumar, N.V., J. Yang, J.K. Pillai, S. Rawat, C. Solano, A. Kumar, M. Grotli, T.L. Stemmler, B.P. Rosen, and
828 M.J. Tamás. 2016. Arsenic directly binds to and activates the yeast AP-1-like transcription
829 factor Yap8. *Mol Cell Biol*. 36:913-922.
830 Lallemand-Breitenbach, V., M. Jeanne, S. Benhenda, R. Nasr, M. Lei, L. Peres, J. Zhou, J. Zhu, B. Raught,
831 and H. de The. 2008. Arsenic degrades PML or PML-RARalpha through a SUMO-triggered
832 RNF4/ubiquitin-mediated pathway. *Nat Cell Biol*. 10:547-555.
833 Lee, J., and D.E. Levin. 2018. Intracellular mechanism by which arsenite activates the yeast stress MAPK
834 Hog1. *Mol Biol Cell*. 29:1904-1915.
835 Lee, J., and D.E. Levin. 2019. Methylated metabolite of arsenite blocks glycerol production in yeast by
836 inhibition of glycerol-3-phosphate dehydrogenase. *Mol Biol Cell*. 30:2134-2140.
837 Lee, J., and D.E. Levin. 2022. Differential metabolism of arsenicals regulates Fps1-mediated arsenite
838 transport. *J Cell Biol*. 221:e202109034.
839 Li, Z., F.J. Vizeacoumar, S. Bahr, J. Li, J. Warringer, F.S. Vizeacoumar, R. Min, B. Vandersluis, J. Bellay,
840 M. Devit, J.A. Fleming, A. Stephens, J. Haase, Z.Y. Lin, A. Baryshnikova, H. Lu, Z. Yan, K. Jin, S.
841 Barker, A. Datti, G. Giaever, C. Nislow, C. Bulawa, C.L. Myers, M. Costanzo, A.C. Gingras, Z.
842 Zhang, A. Blomberg, K. Bloom, B. Andrews, and C. Boone. 2011. Systematic exploration of
843 essential yeast gene function with temperature-sensitive mutants. *Nat Biotechnol*. 29:361-
844 367.
845 Liu, J., B. Chen, R. Zhang, Y. Li, R. Chen, S. Zhu, S. Wen, and T. Luan. 2023. Recent progress in analytical
846 strategies of arsenic-binding proteomes in living systems. *Anal Bioanal Chem*. 415:6915-6929.

Lum, P.Y., C.D. Armour, S.B. Stepaniants, G. Cavet, M.K. Wolf, J.S. Butler, J.C. Hinshaw, P. Garnier, G.D. Prestwich, A. Leonardson, P. Garrett-Engele, C.M. Rush, M. Bard, G. Schimmack, J.W. Phillips, C.J. Roberts, and D.D. Shoemaker. 2004. Discovering modes of action for therapeutic compounds using a genome-wide screen of yeast heterozygotes. *Cell*. 116:121-137.

Marino, S.M., Y. Li, D.E. Fomenko, N. Agisheva, R.L. Cerny, and V.N. Gladyshev. 2010. Characterization of surface-exposed reactive cysteine residues in *Saccharomyces cerevisiae*. *Biochemistry*. 49:7709-7721.

Pan, X., S. Reissman, N.R. Douglas, Z. Huang, D.S. Yuan, X. Wang, J.M. McCaffery, J. Frydman, and J.D. Boeke. 2010. Trivalent arsenic inhibits the functions of chaperonin complex. *Genetics*. 186:725-734.

Panagaki, D., J.T. Croft, K. Keuenhof, L. Larsson Berglund, S. Andersson, V. Köhler, S. Büttner, M.J. Tamás, T. Nyström, R. Neutze, and J.L. Höög. 2021. Nuclear envelope budding is a response to cellular stress. *Proc Natl Acad Sci U S A*. 118:e2020997118.

Parsons, A.B., R.L. Brost, H.M. Ding, Z.J. Li, C.Y. Zhang, B. Sheikh, G.W. Brown, P.M. Kane, T.R. Hughes, and C. Boone. 2004. Integration of chemical-genetic and genetic interaction data links bioactive compounds to cellular target pathways. *Nature Biotechnology*. 22:62-69.

Paul, N.P., A.E. Galvan, K. Yoshinaga-Sakurai, B.P. Rosen, and M. Yoshinaga. 2023. Arsenic in medicine: past, present and future. *Biometals*. 36:283-301.

Peters, R.A., H.M. Sinclair, and R.H. Thompson. 1946. An analysis of the inhibition of pyruvate oxidation by arsenicals in relation to the enzyme theory of vesication. *Biochem J*. 40:516-524.

Rahman, M.A., M.A. Hannan, M.J. Uddin, M.S. Rahman, M.M. Rashid, and B. Kim. 2021. Exposure to Environmental Arsenic and Emerging Risk of Alzheimer's Disease: Perspective Mechanisms, Management Strategy, and Future Directions. *Toxics*. 9:188.

Ramadan, D., P.C. Rancy, R.P. Nagarkar, J.P. Schneider, and C. Thorpe. 2009. Arsenic(III) species inhibit oxidative protein folding *in vitro*. *Biochemistry*. 48:424-432.

Rempel, I.L., M.M. Crane, D.J. Thaller, A. Mishra, D.P. Jansen, G. Janssens, P. Popken, A. Aksit, M. Kaeberlein, E. van der Giessen, A. Steen, P.R. Onck, C.P. Lusk, and L.M. Veenhoff. 2019. Age-dependent deterioration of nuclear pore assembly in mitotic cells decreases transport dynamics. *eLife*. 8:e48186.

Reynolds, E.S. 1963. The use of lead citrate at high pH as an electron-opaque stain in electron microscopy. *J Cell Biol*. 17:208-212.

Sapra, A., D. Ramadan, and C. Thorpe. 2015. Multivalency in the inhibition of oxidative protein folding by arsenic(III) species. *Biochemistry*. 54:612-621.

Schindelin, J., I. Arganda-Carreras, E. Frise, V. Kaynig, M. Longair, T. Pietzsch, S. Preibisch, C. Rueden, S. Saalfeld, B. Schmid, J.Y. Tinevez, D.J. White, V. Hartenstein, K. Eliceiri, P. Tomancak, and A. Cardona. 2012. Fiji: an open-source platform for biological-image analysis. *Nat Methods*. 9:676-682.

Schneider, K.L., X. Hao, K.S. Keuenhof, L.L. Berglund, A. Fischbach, D. Ahmadpour, S. Chawla, P. Gomez, J.L. Hoog, P.O. Widlund, and T. Nystrom. 2024. Elimination of virus-like particles reduces protein aggregation and extends replicative lifespan in *Saccharomyces cerevisiae*. *Proc Natl Acad Sci U S A*. 121:e2313538121.

Shen, S., X.F. Li, W.R. Cullen, M. Weinfeld, and X.C. Le. 2013. Arsenic Binding to Proteins. *Chem Rev*. 113:7769–7792.

Shi, W., J. Wu, and B.P. Rosen. 1994. Identification of a putative metal binding site in a new family of metalloregulatory proteins. *J Biol Chem*. 269:19826-19829.

Soto, C., and S. Pritzkow. 2018. Protein misfolding, aggregation, and conformational strains in neurodegenerative diseases. *Nat Neurosci*. 21:1332-1340.

Tamás, M.J., K.S. Sharma, S. Ibstedt, T. Jacobson, and P. Christen. 2014. Heavy metals and metalloids as a cause for protein misfolding and aggregation. *Biomolecules*. 4:252-267.

Thaller, D.J., and C.P. Lusk. 2018. Fantastic nuclear envelope herniations and where to find them. *Biochem Soc T*. 46:877-889.

898 Thomas, D.J. 2021. Arsenic methylation - Lessons from three decades of research. *Toxicology*.
899 457:152800.
900 Thorsen, M., G. Lagniel, E. Kristiansson, C. Junot, O. Nerman, J. Labarre, and M.J. Tamás. 2007.
901 Quantitative transcriptome, proteome, and sulfur metabolite profiling of the *Saccharomyces*
902 *cerevisiae* response to arsenite. *Physiol Genomics*. 30:35-43.
903 Thorsen, M., G.G. Perrone, E. Kristiansson, M. Traini, T. Ye, I.W. Dawes, O. Nerman, and M.J. Tamás.
904 2009. Genetic basis of arsenite and cadmium tolerance in *Saccharomyces cerevisiae*. *BMC*
905 *Genomics*. 10:105.
906 Vergara-Geronimo, C.A., A. Leon Del Rio, M. Rodriguez-Dorantes, P. Ostrosky-Wegman, and A.M.
907 Salazar. 2021. Arsenic-protein interactions as a mechanism of arsenic toxicity. *Toxicol Appl*
908 *Pharmacol*. 431:115738.
909 Wang, Y., E. Weisenhorn, C.W. MacDiarmid, C. Andreini, M. Bucci, J. Taggart, L. Banci, J. Russell, J.J.
910 Coon, and D.J. Eide. 2018. The cellular economy of the *Saccharomyces cerevisiae* zinc
911 proteome. *Metallomics*. 10:1755-1776.
912 Weids, A.J., and C.M. Grant. 2014. The yeast peroxiredoxin Tsa1 protects against protein-aggregate-
913 induced oxidative stress. *J Cell Sci*. 127:1327-1335.
914 Wing, C.E., H.Y.J. Fung, and Y.M. Chook. 2022. Karyopherin-mediated nucleocytoplasmic transport. *Nat*
915 *Rev Mol Cell Biol*. 23:307-328.
916 Woerner, A.C., F. Frottin, D. Hornburg, L.R. Feng, F. Meissner, M. Patra, J. Tatzelt, M. Mann, K.F.
917 Winklhofer, F.U. Hartl, and M.S. Hipp. 2016. Cytoplasmic protein aggregates interfere with
918 nucleocytoplasmic transport of protein and RNA. *Science*. 351:173-176.
919 Wong, E.D., S.R. Miyasato, S. Aleksander, K. Karra, R.S. Nash, M.S. Skrzypek, S. Weng, S.R. Engel, and
920 J.M. Cherry. 2023. *Saccharomyces* genome database update: server architecture, pan-genome
921 nomenclature, and external resources. *Genetics*. 224:iyac191.
922 Wysocki, R., P.K. Fortier, E. Maciaszczyk, M. Thorsen, A. Leduc, A. Odhagen, G. Owsianik, S. Ulaszewski,
923 D. Ramotar, and M.J. Tamás. 2004. Transcriptional activation of metalloid tolerance genes in
924 *Saccharomyces cerevisiae* requires the AP-1-like proteins Yap1p and Yap8p. *Mol Biol Cell*.
925 15:2049-2060.
926 Wysocki, R., J.I. Rodrigues, I. Litwin, and M.J. Tamás. 2023. Mechanisms of genotoxicity and
927 proteotoxicity induced by the metalloids arsenic and antimony. *Cell Mol Life Sci*. 80:342.
928 Wysocki, R., and M.J. Tamás. 2010. How *Saccharomyces cerevisiae* copes with toxic metals and
929 metalloids. *FEMS Microbiol Rev*. 34:925-951.
930 Yan, X., J. Li, Q. Liu, H. Peng, A. Popowich, Z. Wang, X.F. Li, and X.C. Le. 2016. p-Azidophenylarsenoxide:
931 An Arsenical "Bait" for the In Situ Capture and Identification of Cellular Arsenic-Binding
932 Proteins. *Angew Chem Int Ed*. 55:14051-14056.
933 Zhang, H.N., L. Yang, J.Y. Ling, D.M. Czajkowsky, J.F. Wang, X.W. Zhang, Y.M. Zhou, F. Ge, M.K. Yang, Q.
934 Xiong, S.J. Guo, H.Y. Le, S.F. Wu, W. Yan, B. Liu, H. Zhu, Z. Chen, and S.C. Tao. 2015a. Systematic
935 identification of arsenic-binding proteins reveals that hexokinase-2 is inhibited by arsenic. *Proc*
936 *Natl Acad Sci U S A*. 112:15084-15089.
937 Zhang, T., H. Lu, W. Li, R. Hu, and Z. Chen. 2015b. Identification of Arsenic Direct-Binding Proteins in
938 Acute Promyelocytic Leukaemia Cells. *Int J Mol Sci*. 16:26871-26879.
939 Zhang, X., F. Yang, J.Y. Shim, K.L. Kirk, D.E. Anderson, and X. Chen. 2007. Identification of arsenic-
940 binding proteins in human breast cancer cells. *Cancer Lett*. 255:95-106.
941 Zhang, X.W., X.J. Yan, Z.R. Zhou, F.F. Yang, Z.Y. Wu, H.B. Sun, W.X. Liang, A.X. Song, V. Lallemand-
942 Breitenbach, M. Jeanne, Q.Y. Zhang, H.Y. Yang, Q.H. Huang, G.B. Zhou, J.H. Tong, Y. Zhang, J.H.
943 Wu, H.Y. Hu, H. de The, S.J. Chen, and Z. Chen. 2010. Arsenic trioxide controls the fate of the
944 PML-RARalpha oncoprotein by directly binding PML. *Science*. 328:240-243.
945 Zhou, X., A. Arita, T.P. Ellen, X. Liu, J. Bai, J.P. Rooney, A.D. Kurtz, C.B. Klein, W. Dai, T.J. Begley, and M.
946 Costa. 2009. A genome-wide screen in *Saccharomyces cerevisiae* reveals pathways affected by
947 arsenic toxicity. *Genomics*. 94:294-307.
948 Zhou, X., X. Sun, K.L. Cooper, F. Wang, K.J. Liu, and L.G. Hudson. 2011. Arsenite interacts selectively
949 with zinc finger proteins containing C3H1 or C4 motifs. *J Biol Chem*. 286:22855-22863.

950 Zhou, Y., B. Zhou, L. Pache, M. Chang, A.H. Khodabakhshi, O. Tanaseichuk, C. Benner, and S.K. Chanda.
951 2019. Metascape provides a biologist-oriented resource for the analysis of systems-level
952 datasets. *Nature Commun*. 10:1523.
953

1A.

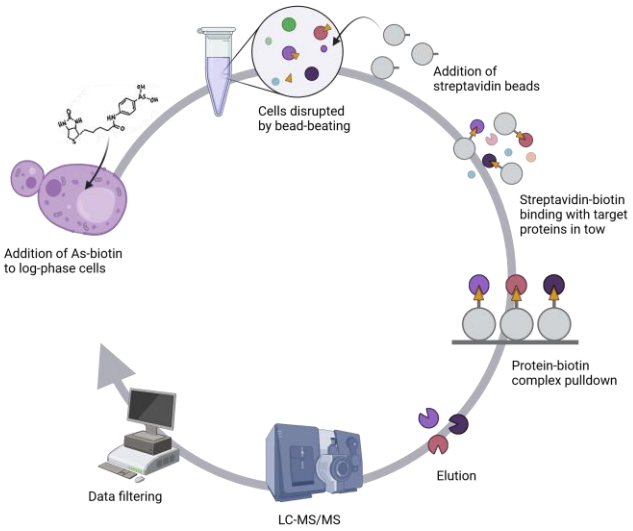

1B.

Percentage proteins with cysteine			Mean no. cysteine motifs per protein	
Cysteine motif	As-binding	Proteome	As-binding	Proteome
C	99.4%***	90.7%	10.4***	6.3
CC	35.1%***	12.1%	0.39***	0.14
CxC	12.6%*	9.7%	0.14	0.12
CxxC	21.3%*	16.0%	0.25	0.27
CxxxC	16.7%**	10.4%	0.19	0.13

1C.

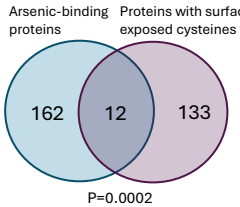

1D.

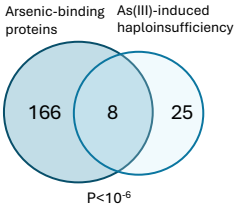

1E.

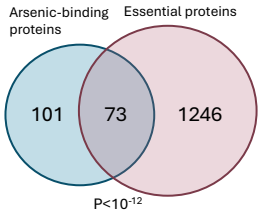

1F.

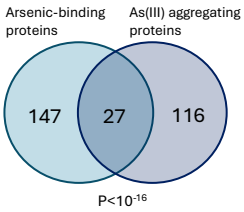

2A.

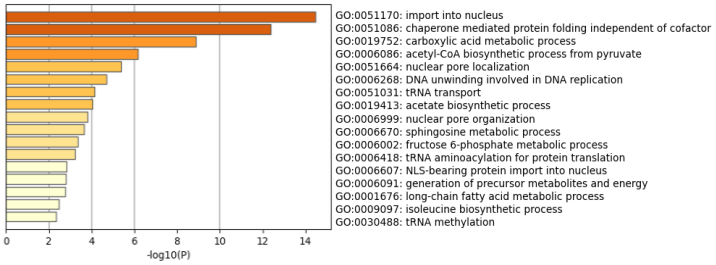

2B.

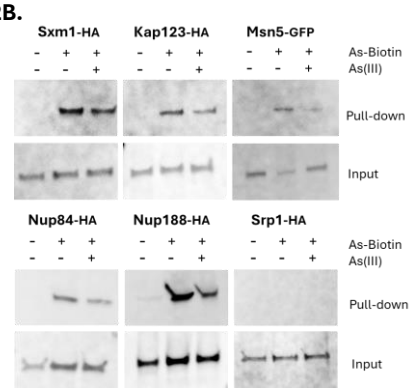

2C.

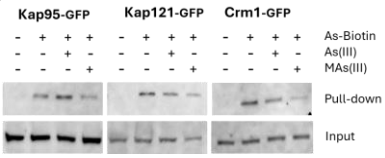

2D.

Protein	Cysteine content	Motifs
Srp1	8 (1.47%)	-
Kap95	11 (1.27%)	CXC
Kap121	15 (1.38%)	CC, CXXC
Kap123	9 (0.08%)	-
Sxm1	11 (1.16%)	CXC
Crm1	12 (1.09%)	-
Msn5	23 (1.85%)	CC, CXXXC, CXXXXC
Nup84	7 (1.0%)	CXXXC
Nup188	12 (0.7%)	CC, CXXXXC

3A.

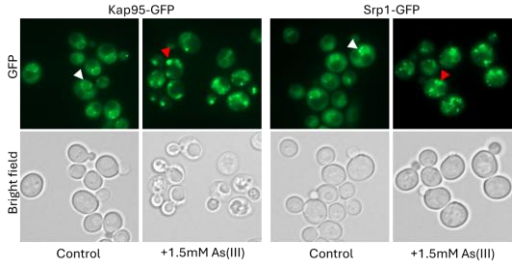

3B.

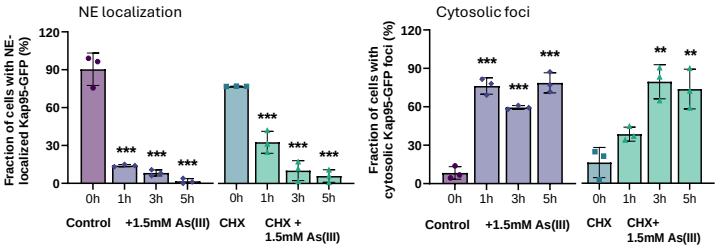

3D.

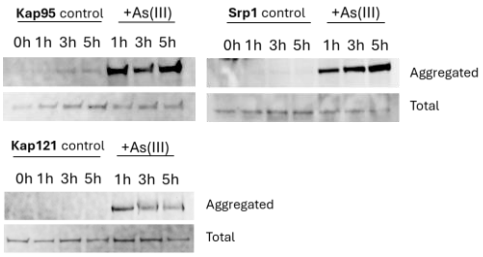

3C.

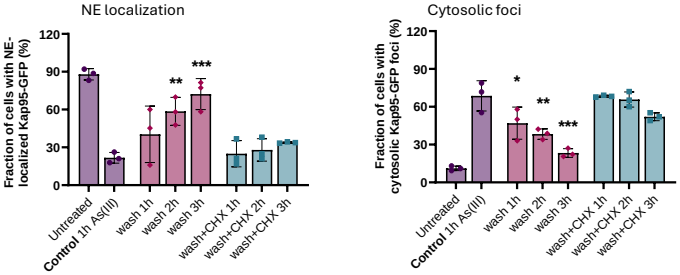

4A.

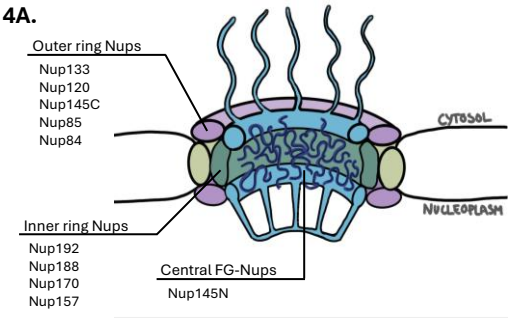

4C.

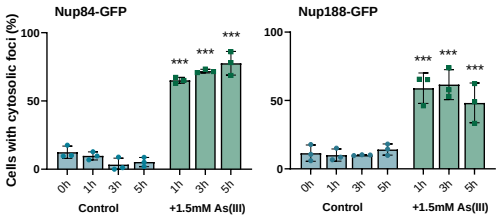

4B.

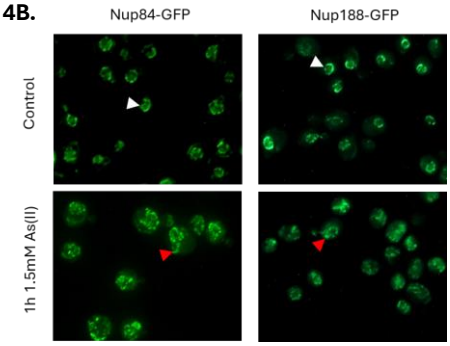

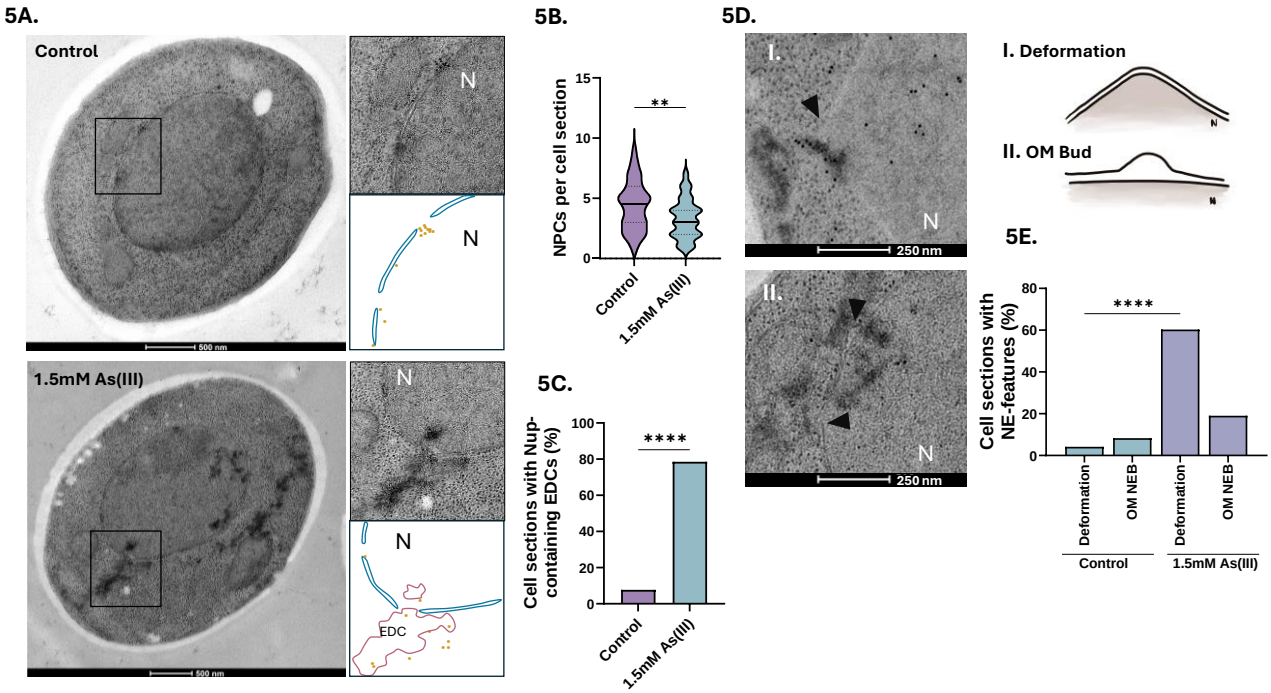
5A.
Control
N
N
1.5mM As(III)
N
N
EDC
5B.
NPCs per cell section
**
Control
1.5mM As(III)
5C.
Cell sections with Nup-containing EDCs (%)
****
Control
1.5mM As(III)
5D.
I.
N
250 nm
II.
N
250 nm
I. Deformation
II. OM Bud
5E.
Cell sections with NE-features (%)
****
Deformation
OM NEB
Deformation
OM NEB
Control
1.5mM As(III)

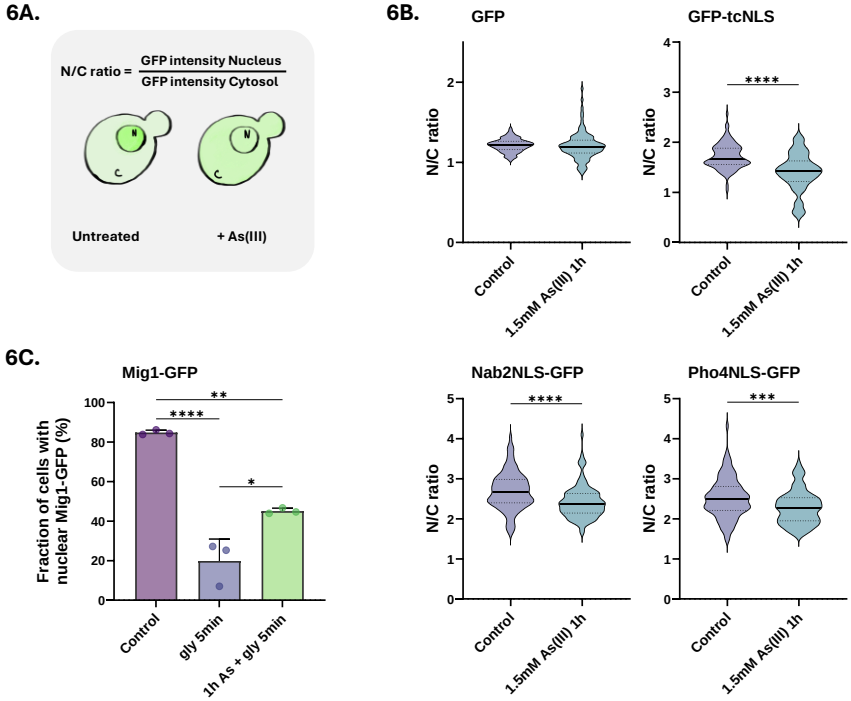
6A.
N/C ratio = GFP intensity Nucleus / GFP intensity Cytosol
Untreated
+ As(III)
6B.
GFP
GFP-tcNLS
N/C ratio
****
Control
1.5mM As(III) 1h
6C.
Mig1-GFP
Fraction of cells with nuclear Mig1-GFP (%)
**
****
*
Control
gly 5min
1h As + gly 5min
Nab2NLS-GFP
Pho4NLS-GFP
N/C ratio
****
***
Control
1.5mM As(III) 1h

7.

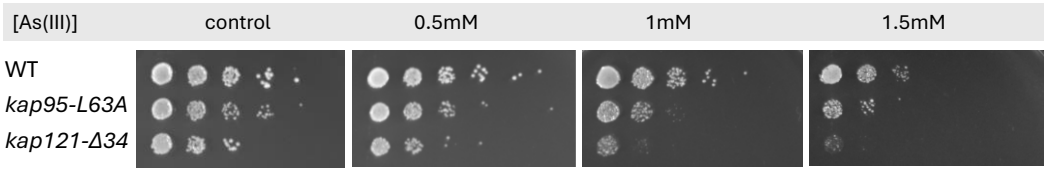
[As(III)]
control
0.5mM
1mM
1.5mM
WT
kap95-L63A
kap121-Δ34

S1.

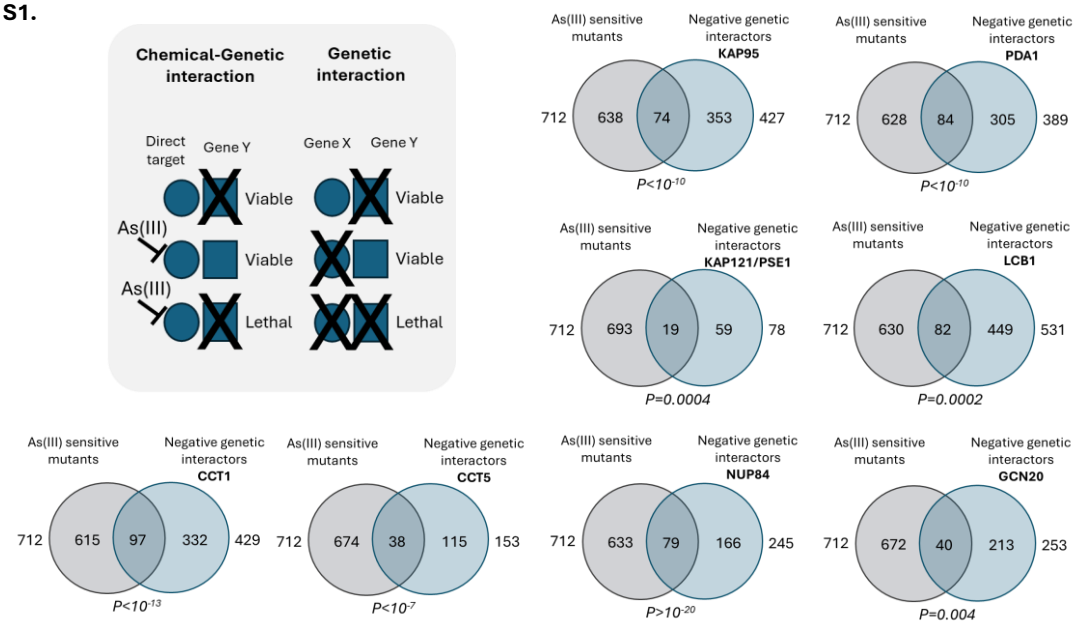
Chemical-Genetic interaction
Genetic interaction
Direct target
Gene Y
Gene X
Gene Y
Viable
Viable
As(III)
Viable
Viable
As(III)
Lethal
Lethal
As(III) sensitive mutants
Negative genetic interactors
KAP95
712
638
74
353
427
P<10-10
As(III) sensitive mutants
Negative genetic interactors
PDA1
712
628
84
305
389
P<10-10
As(III) sensitive mutants
Negative genetic interactors
KAP121/PSE1
712
693
19
59
78
P=0.0004
As(III) sensitive mutants
Negative genetic interactors
LCB1
712
630
82
449
531
P=0.0002
As(III) sensitive mutants
Negative genetic interactors
CCT1
712
615
97
332
429
P<10-13
As(III) sensitive mutants
Negative genetic interactors
CCT5
712
674
38
115
153
P<10-7
As(III) sensitive mutants
Negative genetic interactors
NUP84
712
633
79
166
245
P>10-20
As(III) sensitive mutants
Negative genetic interactors
GCN20
712
672
40
213
253
P=0.004

S2. **Srp1 (Kap60)**

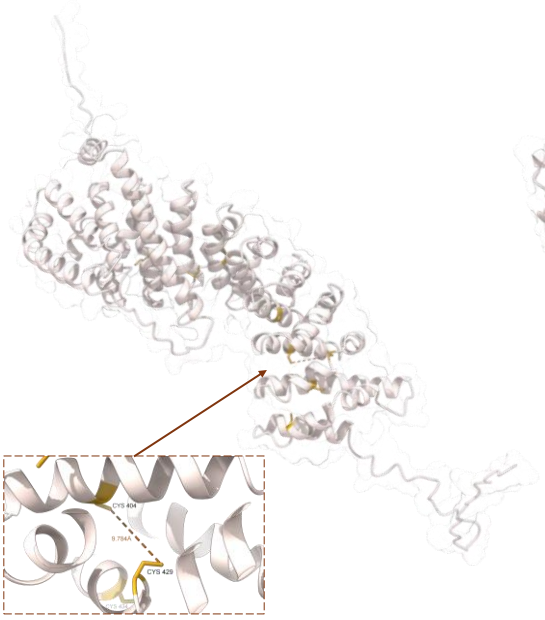

C404-429 9.784Å

Kap95

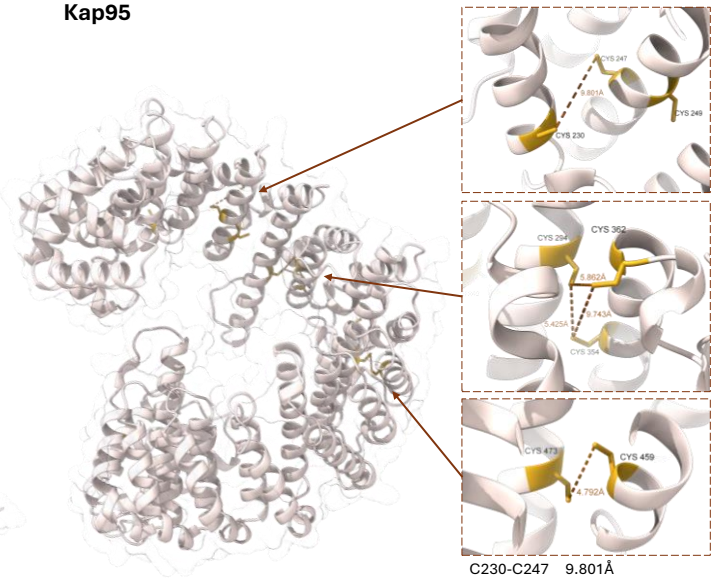

C230-C247 9.801Å

C294-C354 5.425Å
C294-C362 5.862Å
C354-C362 9.743Å

C459-C473 4.792Å

S2. **Kap121(Pse1)**

C428-C429 5.758Å
C429-C463 7.785Å

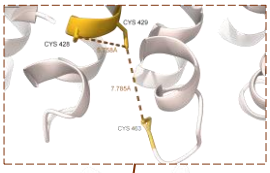

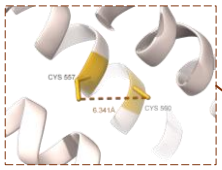

C557-C560 6.341Å

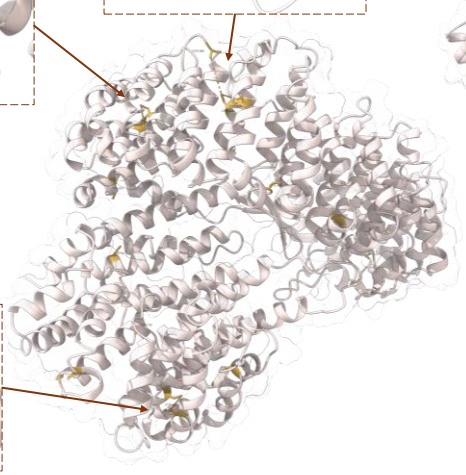

C927-C939 5.099Å

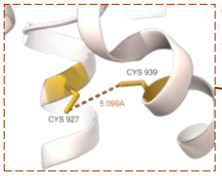

Crm1 (Xpo1)

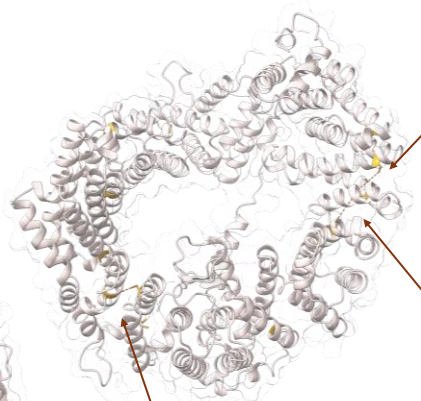

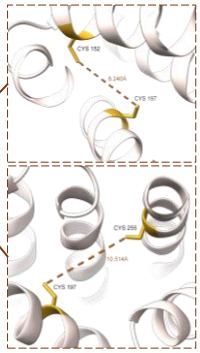

C152-C197 8.240Å
C294-C354 10.514Å

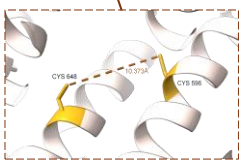

C294-C362 10.373Å

S2. Kap123 **Kap108(Sxm1)**

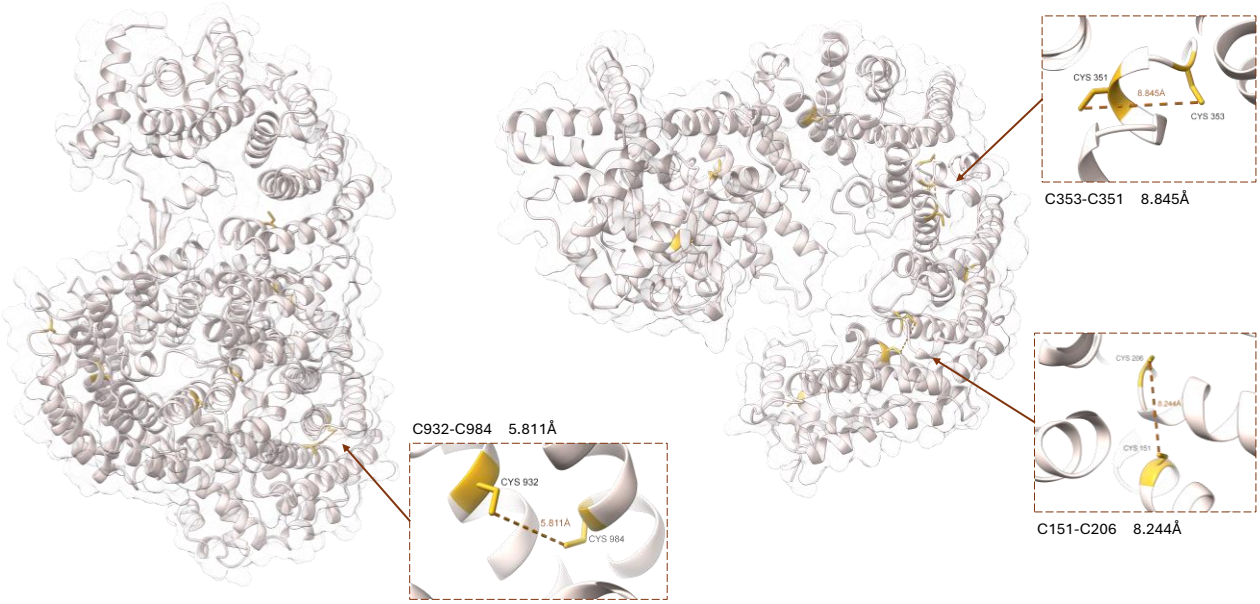

S2. Msn5

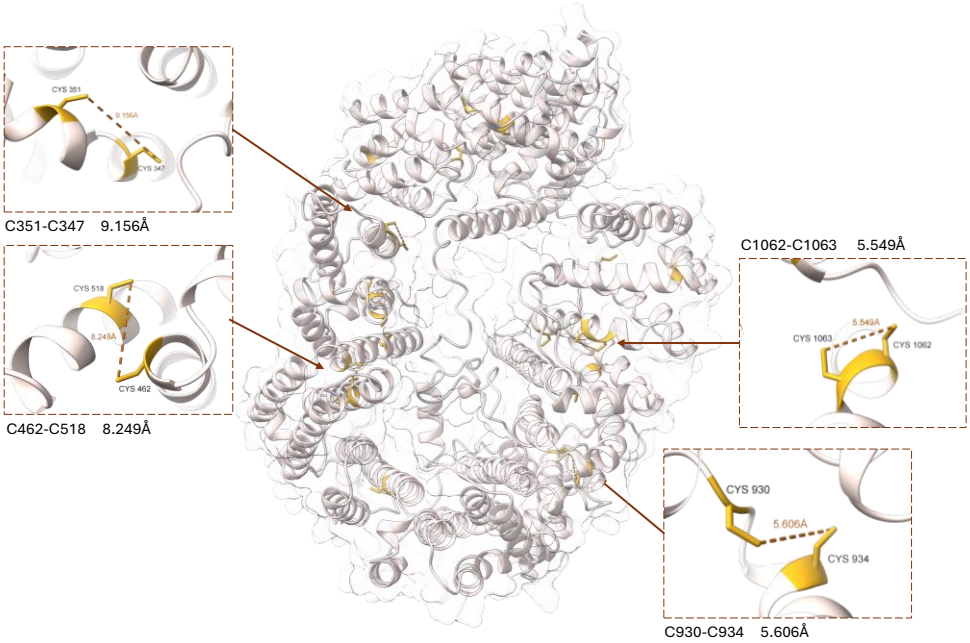

S2. **Nup84** **Nup188**

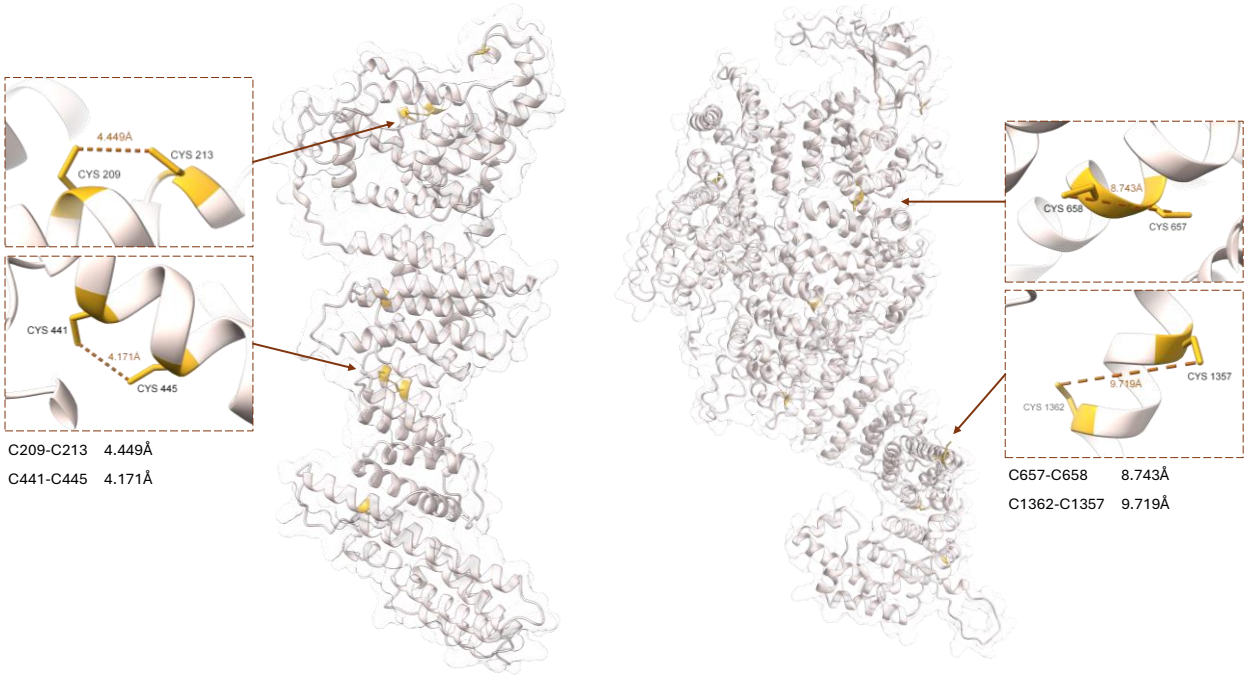

S3A.

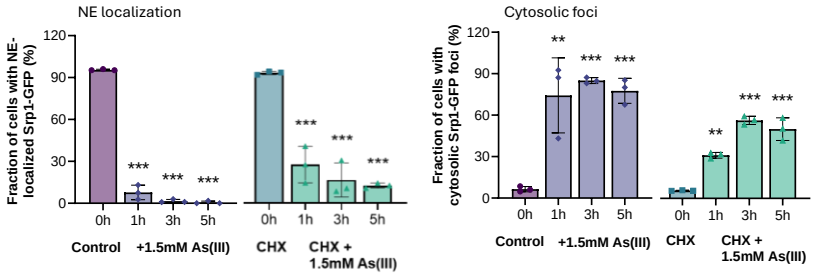

S3B.

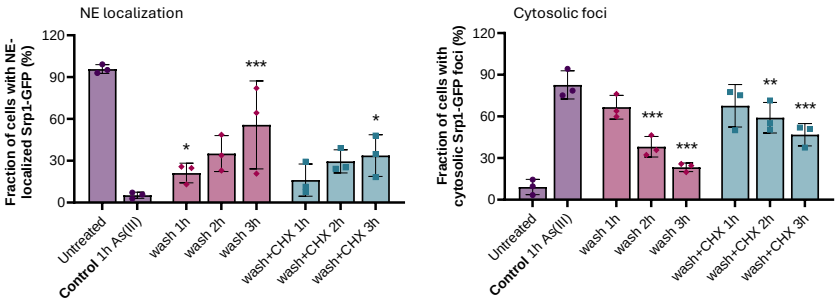

S4A.

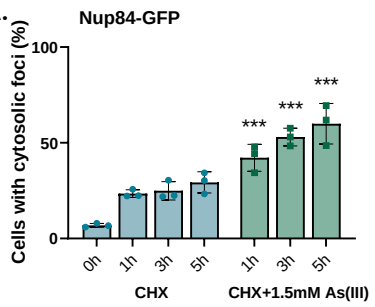
Nup84-GFP
Cells with cytosolic foci (%)
100
50
0
***
***
***
0h
1h
3h
5h
1h
3h
5h
CHX
CHX+1.5mM As(III)

S4B.

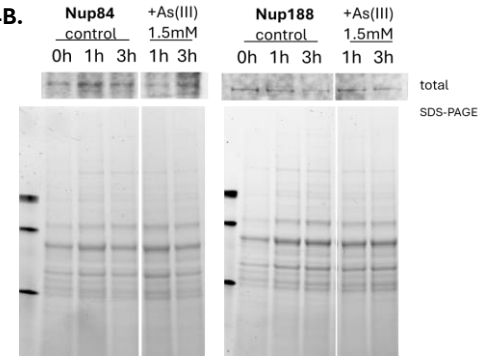
Nup84
control
+As(III)
1.5mM
0h 1h 3h 1h 3h
Nup188
control
+As(III)
1.5mM
0h 1h 3h 1h 3h
total
SDS-PAGE

S5.

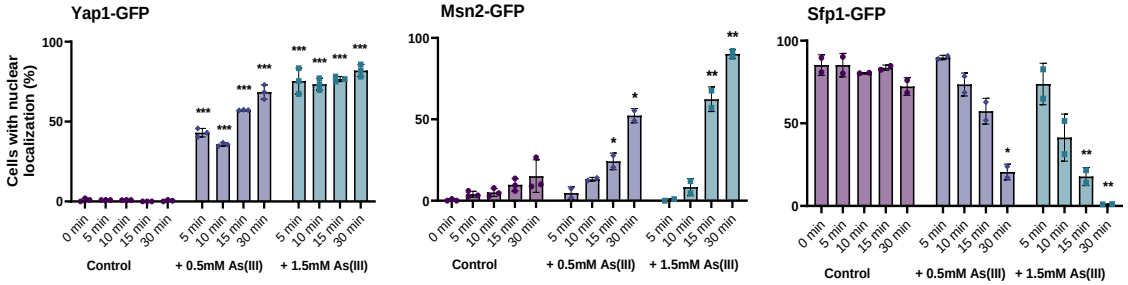
Yap1-GFP
Msn2-GFP
Sfp1-GFP
Cells with nuclear localization (%)
100
50
0
0 min
5 min
10 min
15 min
30 min
Control
+ 0.5mM As(III)
+ 1.5mM As(III)